University of California, Santa Barbara
Departments of Mechanical Engineering and Materials

Characterization of Lightweight Ceramic Ablator Materials

NASA Ames Research Center
Thermal Protection Materials and Systems Branch

Principal Investigators: K. Parmenter and F. Milstein
Graduate Student Research Assistants: A. DiCarlo and R. Lotz
Undergraduate Laboratory Assistants: J. Mencher, E. Guerra, C. Luna and P. Valenzuela

National Aeronautics and Space Administration
Research Grants NAG 2-1148 and NCC 2-1049

February 4, 1999

(NB FIG 4.11 & 4.12, pg 51 — need correction.)

Table of Contents

Executive Summary

This report presents the results of work carried out on NASA grants NAG 2-1148 and NCC 2-1049. Work on the latter grant is also continuing, and additional results will be presented in a subsequent report. Numerous experimental studies of the mechanical responses and microstructures of Lightweight Ceramic Ablator (LCA) materials were completed; additional mechanical testing and microscopy evaluation is currently underway. The specific LCA materials subjected to testing included SIRCA 15A, SIRCA 15F, and PICA, in both their "virgin" and "charred" forms. Additionally, some testing was done on the respective substrate materials, AIM, FRCI, and Fiberform.

Mechanical testing included hardness measurement, determination of the stress-strain response during compression, and shear testing by the Iosipescu shear test procedure. For each type of test, measurements were done with the load applied parallel to the preferred fiber orientation (referred to as "in-plane" testing) and perpendicular to the preferred fiber orientation ("out-of-plane" testing). Numerical values of hardness, compressive strength, and elastic moduli were obtained for both orientations. During shear testing, the samples failed in a tensile or bending mode before the shear stress, that would have caused a shear failure, was reached. Thus, shear testing provided a "lower bound" to the "true shear strength," wherein the "true" value is certainly higher.

The characteristic in-plane and out-of-plane mechanical responses were markedly different. For example during in-plane compressive loading, the materials failed by an apparent "separation and buckling" mechanism. By contrast, under out-of-plane compression, the materials underwent significant, highly nonlinear, plastic (i.e., permanent) deformation, wherein the stress (and its rate of change) increased with increasing strain. Considerable energy was absorbed during out-of-plane compression. This behavior is readily understood from microstructural considerations.

A number of fracture surfaces of samples that underwent compressive testing were viewed with a Scanning Electron Microscope (SEM). Initial microscopy results include surface images of charred SIRCA 15A, virgin SIRCA 15F, and virgin PICA. Fracture surfaces were viewed in directions parallel and perpendicular to the fiber "planes," at magnifications ranging from X15 to X10000.

Chapter

1

Background

Families of materials called Lightweight Ceramic Ablators (LCAs) have been developed at the Thermal Protection Materials and Systems Branch, NASA Ames Research Center *(Tran [1994])*, for use on planetary missions that require a heat shield able to withstand very high heating rates and shear loads, while providing the necessary thermal protection for the interior of the vehicle. LCAs, in general, consist of highly porous fibrous ceramic substrates partially impregnated with organic resins. Examples include Phenolic Impregnated Carbon Ablator (PICA) and Silcone Impregnated Reusable Ceramic Ablator (SIRCA). PICA was chosen to be the heat shield material for the forebody of the Stardust sample return capsule *(Tran, et al. [1997a])*. It is also base-lined for the 5th discovery mission (Genesis), and is being considered for the Mars 2005 sample return capsule *(Marschall and Cox [1999])*. SIRCA was used as the heat shield on the aft-plate of the Mars Pathfinder *(Tran, et al. [1995])*, and was chosen to be used on the leading edges and nose cap of the X-34 vehicle *(Marschall and Cox [1999])*.

In order to optimize the development and use of LCAs, it is necessary to measure the properties and behaviors of these materials, including the thermophysical, thermochemical, mechanical, and microstructural characteristics, and to obtain fundamental scientific understanding of the bases for these properties. Tran and coworkers *([1996a,b; 1997a,b])* have carried out extensive thermal performance and ablation characteristic measurements, including arc-jet testing. More recently Marschall and coworkers measured the gas permeability of several rigid fibrous refractory insulations *(Marschall and Milos [1998])* and PICA and SIRCA LCA materials *(Marschall and Cox [1999])*. Arc-jet testing revealed materials that can withstand very high heating rates and surface pressures and that are more mass efficient than most traditional ablative materials.

At the University of California, Santa Barbara, PI (F. Milstein), along with postdoctoral researcher (K. Parmenter), graduate students (A. DiCarlo and R. Lotz), lab assistant (J. Mencher), and summer interns (E. Guerra, C. Luna, and P. Valenzuela), has carried out experimental studies of mechanical properties of the LCAs that are of interest to NASA

under NASA grants NAG 2-1148 and NCC 2-1049. Experimental work focused on hardness, compressive strength, and shear strength of PICA and SIRCA material. Both "FRCI" and "AIM" types of SIRCA material were investigated. Additionally, electron microscopic characterizations were made. This report presents the findings of these investigations to date; as such, it represents the final report on NAG 2-1148 combined with a report of work in progress on NCC 2-1049.

Chapter

2

Materials

Details of the procedures for processing PICA and SIRCA materials may be found in references *[1996a], [1996b],* and *[1997]* by Tran, et al. PICA consists of a fibrous carbon substrate called Fiberform® manufactured by Fiber Materials, Inc., and phenolic resin infiltrant. The basic process consists of chopping carbon fibers (14-16 μm diameter, 1600 μm length) in a water slurry, adding a soluble phenolic resin to the mixture and vacuum casting. The resulting billet is dried, resin cured, and carbonized to 1440 °F, and subsequently heat treated at 3240 °F. The final density of PICA used in the present study ranged from approximately 210 to 230 kg/m^3 (13 to 14 lbm/ft^3).

Two types of SIRCA material were investigated in this study. The first type (SIRCA 15A) consists of Ames Insulation Material (AIM) as the substrate and silicone resin as the infiltrant. The AIM substrate materials are made from all silica fibers (~ 3 μm diameter). The "15" in the name of this material indicates its approximate density in lbm/ft^3, and the "A" denotes the AIM type of substrate. The second type of SIRCA material tested (SIRCA 15F) consists of Fibrous Refractory Composite Insulation (FRCI) as the substrate and silicone resin as the infiltrant. The FRCI substrate materials are made from 78% silica fibers (~ 3 μm diameter), 20% Nextel 312 fibers (~ 8 μm diameter), and 2% SiC *(Johnson [1999])*. The Nextel 312 fibers consist of 62% Al_2O_3, 14% B_2O_3, and 4% SiO_2 *(Johnson [1999]*. Once again, the "15" in the name of this material indicates its approximate density in lbm/ft^3, and the "F" denotes the FRCI type of substrate. The approximate final density ranges of SIRCA used in the current study were 300 to 320 kg/m^3 (19 to 20 lbm/ft^3) for SIRCA 15A, and 240 to 260 kg/m^3 (15 to 16 lbm/ft^3) for SIRCA 15F.

During processing, the fibers in the SIRCA and PICA materials tend to align themselves normal to a pressing direction *(Marschall and Cox [1999])*. For simplicity, one can view these materials as having layers of fibers (or "planes") that are randomly oriented within a given layer. A simplified diagram of the fiber planes is provided in Figure 2.1. In reality, the fiber arrangement is more complex, with a certain percentage of fibers aligning themselves vertically, or at an angle with respect to the horizontal plane. The fibers do

not actually congregate in individual planes. The planar concept, however, simplifies, and captures the essence of, the anisotropic nature of these materials. Owing to this anisotropy, mechanical tests were done in both the "in-plane" and "out-of-plane" directions. The "in-plane" direction refers to a loading direction that is parallel to the fiber planes, and the "out-of-plane" direction refers to a loading direction that is perpendicular to the fiber planes.

During planetary entry, protective heat shields are exposed to high heating rates and high shear loads. The LCA materials develop a char layer as the surfaces ablate in these extreme environments *(Tran, et al. [1996a,b; 1997a,b])*. At the NASA Ames Research Center planetary entry is simulated in two arc-jet facilities, the 60 MW Interaction Heating Facility and the 20 MW Aerodynamic Heating Facility. Materials tested in the arc-jet facilities ablate and develop char layers, as they would during planetary entry. The char layer that results from such a test has properties that vary with surface depth. The fact that the properties are variable presents a mechanical testing difficulty. In order to avoid this problem, materials that were uniformly charred throughout the thickness were obtained by pyrolyzing virgin materials in an oven. The "charring" was done in a tube furnace at 1000°C in an argon environment. The material is put into the oven and the temperature is ramped to 1000°C and held at 1000°C for 10 minutes. It is then cooled to room temperature *(Johnson [1999])*.

In addition to the "as-cast" PICA and SIRCA materials (which are refered to as "virgin" materials) charred PICA and SIRCA materials were investigated, as well. For the case of hardness experiments, materials were tested that had been charred in the arc-jet facility (which yielded variable material properties). For compression and shear experiments, materials were tested that had been "oven-charred" with the pyrolysis process (with uniform properties). The approximate final densities for "oven-charred" materials are 220 kg/m^3 (14 lbm/ft^3) for PICA, 240 kg/m^3 (15 lbm/ft^3) for SIRCA 15A, and 250 kg/m^3 (16 lbm/ft^3) for SIRCA 15F.

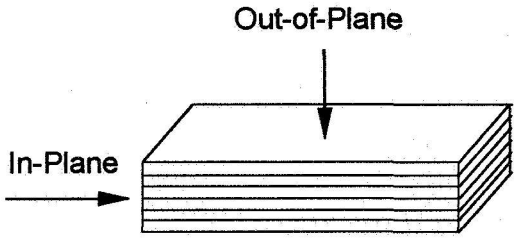

Figure 2.1

Simplified schematic illustration of fiber "planes" in SIRCA and PICA materials. The arrows show the direction of applied load with respect to the fiber orientation during the application of an "in-plane" and an "out-of-plane" load.

Chapter

3

Hardness Testing

The LCAs comprise new material systems with nontraditional mechanical properties. In some cases, traditional or standard mechanical testing procedures will work well; in other cases, new test procedures need to be tried and verified. For example, among our goals is the development of simple, relatively non-destructive tests (e.g. hardness or microhardness indentation) to evaluate the yield and the ultimate strength of LCAs without necessarily stressing the materials to the point where damage is induced. Such relationships between strength and hardness are well known in metals and alloys. The PI and one of his former students (K. Kim) showed such a relation to occur for polymer concrete materials *(Kim and Milstein [1987])*. More recently, in work done for NASA Ames Research Center, a relation between hardness and compressive strength was established for silica aerogels, including those that were fiber-reinforced *(Parmenter and Milstein [1998])*. Similarly, it has been shown that various other properties, including electronic properties of radiation detector semiconductors, correlate well with microhardness *(Schieber, et al. [1989], Georgeson and Milstein [1989], and James et al. [1992])*.

In our initial work with the LCAs, while we found standard compression testing to be an effective material characterization technique, standard micro- and macro-hardness tests did not yield meaningful results. This is because surface features of LCAs, such as fibers and pores, are of the same order of size as micro-indenters, and loads for macroindentation tests are too large. Thus, LCAs require non-traditional hardness tests that do not cause macroscopic cracking and are representative of the entire composite.

This was accomplished at low loads with a spherical indenter with large radius compared to material surface features. The indenter was a 19.05 mm diameter steel ball, and loads were approximately 30 N and smaller. The ball was inserted into the socket fixture which was secured to the crosshead of a displacement-controlled *Instron 1123* testing machine. The load was measured with a compression load cell, and the crosshead displacement was measured with a linear variable differential transformer (LVDT). Crosshead speed was 0.102 mm/min. All tests were conducted under ambient conditions. The virgin

material surfaces were sanded with 400 "grit" sand paper and dusted with compressed air. The charred surfaces were undisturbed. An initial preload of 1.0 N was applied to minimize surface effects. The load was subsequently applied to the full-loading value and then reduced to the preload value where the depth of penetration, δ, was determined. Figure 3.1 graphically depicts the depth, δ, on a Load versus Displacement curve for a typical hardness test. The indent surface area, A, was approximated from the measured value of δ and ball diameter, D, with the relationship $A = \pi D\delta$. The hardness, H, was defined as the maximum load, L_{max}, divided by the indent surface area, $H = L_{max}/A$.

Three types of LCAs (SIRCA 15A, SIRCA 15F, and PICA) were tested for hardness in both the in-plane direction and the out-of-plane direction. A limited number of indents were also made on surfaces that had been charred in NASA Ames' Arc Jet Facility. The charred surfaces were parallel to the fiber planes, and thus the indents were made in the out-of plane direction. The "in-plane" direction refers to a loading direction that is parallel to the fiber planes, and the "out-of-plane" direction refers to a loading direction that is perpendicular to the fiber planes, as illustrated in Figure 2.1. In addition, the three types of un-impregnated material (AIM, FRCI, and Fiberform) that are the corresponding fibrous substrates for SIRCA 15A, SIRCA 15F and PICA, respectively, were tested for hardness in the in-plane and out-of plane directions for comparison with the LCAs. The purpose for comparing the fibrous substrates with the impregnated composites was to quantify how much of the material's compressive strength is attributed to the substrate, and how much results from the impregnation process.

Examples of load-displacement curves during hardness testing of SIRCA 15A, SIRCA 15F and PICA are shown in Figures 3.2-3.4. The calculated hardness values of the three types of LCAs are listed in Table 3.1. Virgin SIRCA 15A and PICA responded well to a peak load of 30 N, and thus all of the indents on these materials were made with a nominal 30 N peak load. The virgin SIRCA 15F material began to crack in some cases at loads greater than 20 N, resulting in choppy load-displacement curves. Therefore, half of the indents were tested with nominal peak loads of 20 N and the other half with nominal peak loads of 30 N. Charred SIRCA 15F and PICA were loaded nominally to 20 N, and Charred SIRCA 15A to 20 N for half of the indents, and 30 N for the other half.

Results indicate that all three type of LCAs are more compliant in the out-of-plane direction compared with the in-plane direction as evidenced by the smaller slopes in the Load versus Displacement curves for the out-of-plane direction. This is consistent with the behavior of transversely isotropic fiber composites. All three types of LCAs are also

softer in the out-of-plane direction compared with the in-plane direction. That is, the respective average hardness values in the out-of-plane direction for SIRCA 15A, SIRCA 15F, and PICA are 1.66 MPa, 1.39 MPa, and 1.45 MPa; whereas, the average hardness values in the in-plane direction are 2.45 MPa, 2.37 MPa, and 1.81 MPa, respectively.

The hardness values of the charred out-of-plane surface compared to the virgin out-of-plane surface were larger in the case of SIRCA 15F (2.60 MPa compared with 1.39 MPa). But the hardness values for the charred versus virgin out-of-plane surfaces were comparable in the case of SIRCA 15A (1.64 MPa compared with 1.66 MPa), and were smaller in the case of PICA (0.58 MPa compared with 1.45 MPa). (However, it should be mentioned that the charred PICA results are limited to one indent; conclusions from such limited data are made with extreme caution. Additional studies of charred material are being carried out currently to obtain a larger data base upon which to draw reliable conclusions.)

The standard deviations for hardness tests varied from 6% deviation in the best case (SIRCA 15A, out-of-plane) to 20% deviation in the worst case (SIRCA 15A, charred). Larger deviations in the charred SIRCA 15A could be attributed to a load dependence of the char layer, which, in turn, could be caused by a gradient in the mechanical properties of the char layer. No appreciable load dependence was observed for the hardness of the virgin SIRCA 15F material between about 20 N and 30 N. However, there would be a tendency for the apparent measured hardness to decrease at loads higher than 30 N due to cracking and surface cave-ins. This is particularly true for SIRCA 15F tested in the in-plane direction.

Representative load versus displacement curves for the fibrous substrate materials AIM, FRCI, and Fiberform are provided in Figures 3.5-3.7. All tests were done with a peak load of approximately 30 N. Calculated hardness values for the in-plane and out-of-plane directions are listed in Table 3.2.

The results indicate that the AIM material is approximately one-fourth as hard as the SIRCA 15A material in both the in-plane direction (0.59 MPa compared with 2.45 MPa) and out-of-plane direction (0.41 MPa compared with 1.66 MPa). The hardness values of the FRCI material and the SIRCA 15F material are roughly equivalent. The Fiberform material is about two-fifths as hard as the PICA material in both the in-plane direction (0.67 MPa compared with 1.81 MPa) and out-of-plane direction (0.57 MPa compared with 1.45 MPa). It is interesting that essentially the full "compressive strength " (as indicated

by hardness testing) of the SIRCA 15F appears to be inherent in the compressive strength of the fibrous substrate, whereas impregnation with the polymer "fillers" serves to considerably strengthen SIRCA 15A and PICA.

Another interesting result is that the hardness of Fiberform in the out-of-plane direction (0.57 MPa) is comparable to the hardness of charred PICA in the out-of-plane direction (0.58 MPa). This may be explained by the fact that, when viewed with an optical microscope, the top-most surface of charred PICA appears to consist of a fibrous matrix alone, with the phenolic having been ablated. The charred top surface may therefore have properties similar to Fiberform.

Figure 3.1
Load versus displacement curve for a typical hardness test.
δ is the measured depth after subjecting the specimen to the maximum load L_{max}, and returning the load to the preload value of 1.0 N.

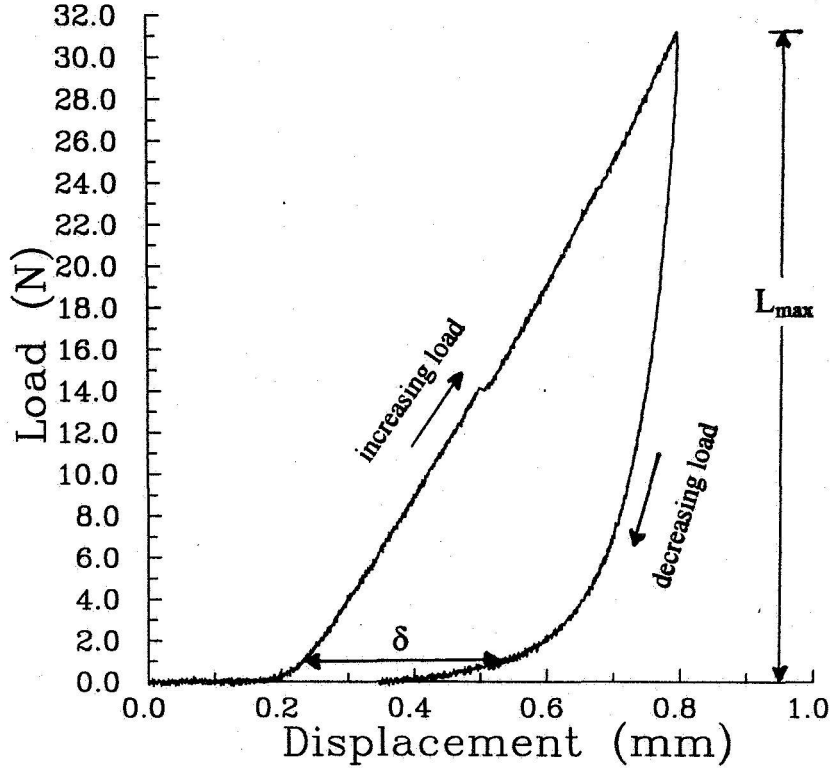

Figure 3.2
Representative load-displacement curves during hardness indentation for virgin SIRCA 15A in the in-plane and out-of-plane directions, and for charred SIRCA 15A in the out-of-plane direction.

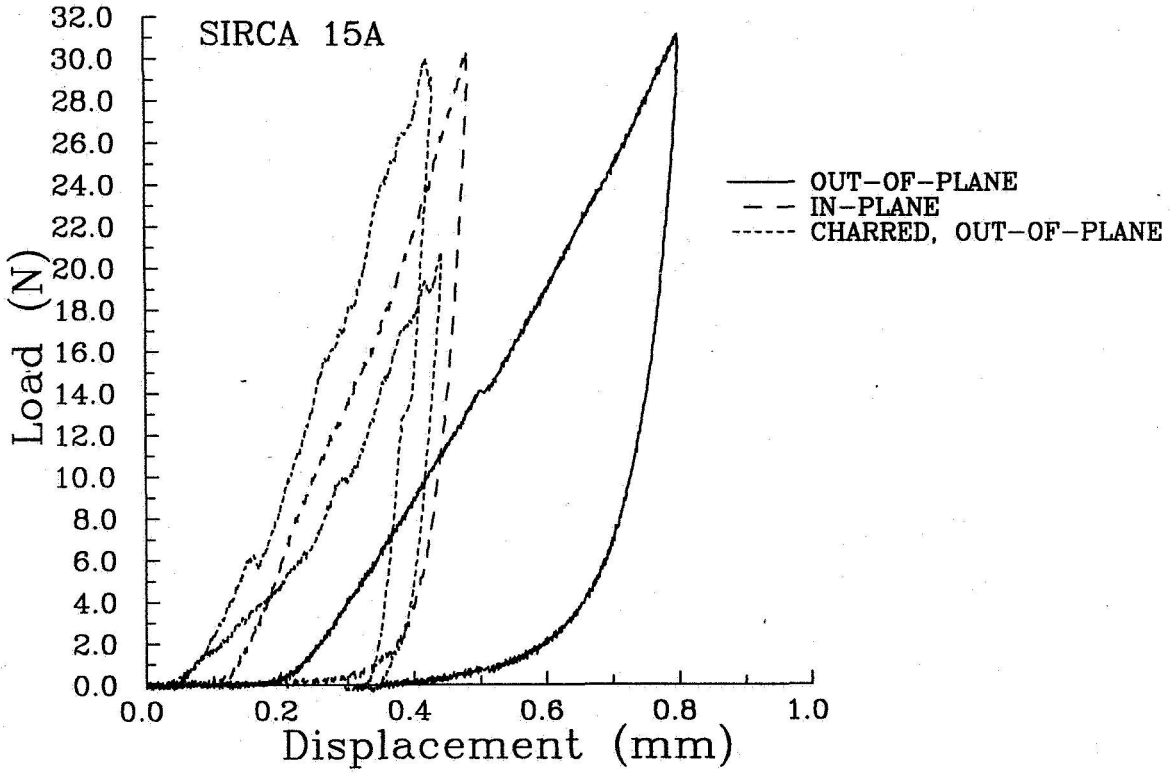

Figure 3.3
Representative load-displacement curves during hardness indentation for virgin SIRCA 15F in the in-plane and out-of-plane directions, and for charred SIRCA 15F in the out-of-plane direction.

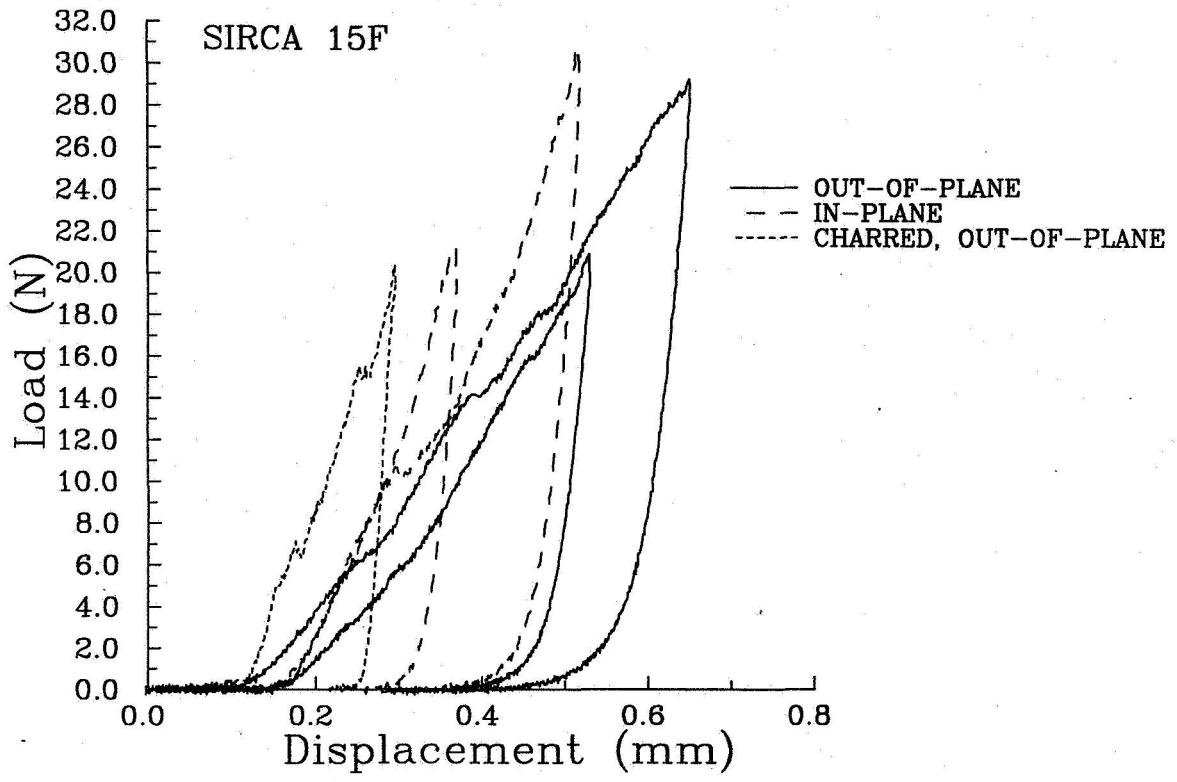

Figure 3.4
Examples of load-displacement curves during hardness indentation for virgin PICA in the in-plane and out-of-plane directions, and for charred PICA in the out-of-plane direction.

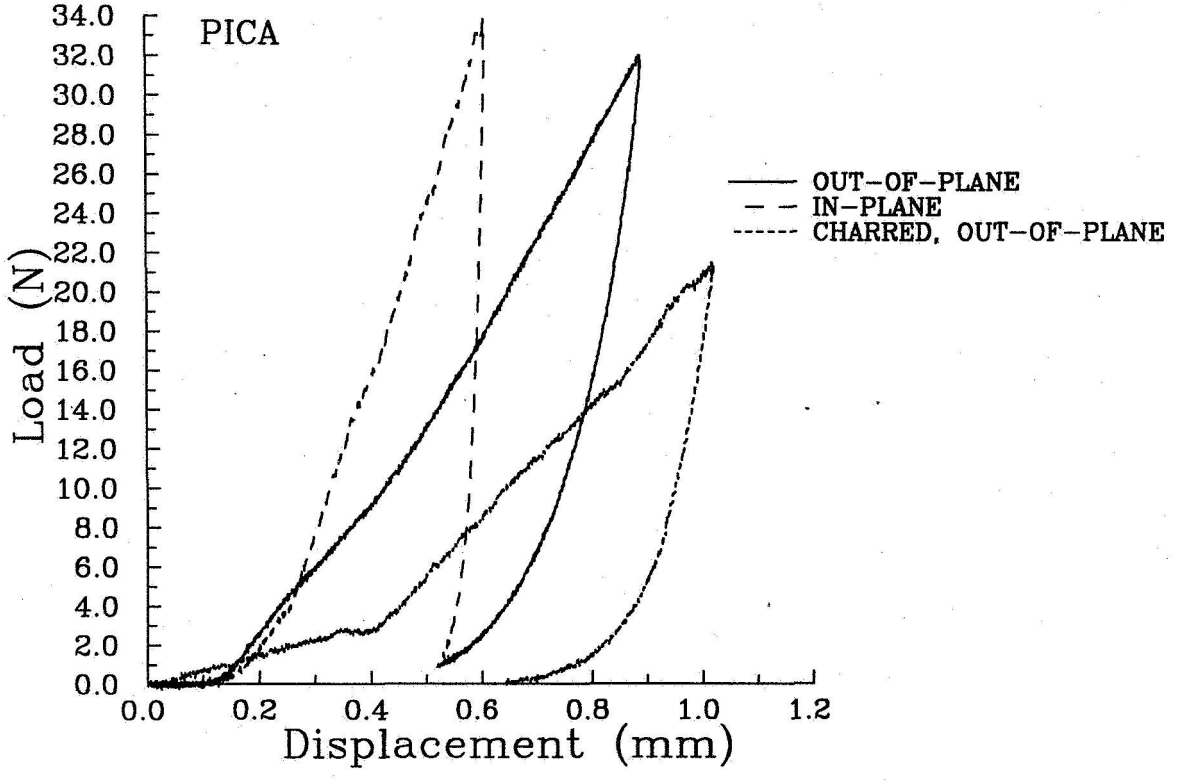

Table 3.1
Hsardness values for virgin LCAs in the in-plane and out-of-plane directions, and for charred LCAs in the out-of-plane direction.

	SIRCA 15A			SIRCA 15F			PICA		
	out-of-plane	in-plane	charred	out-of-plane	in-plane	charred	out-of-plane	in-plane	charred
test #	H (MPa)	H (MPa)	H (MPa)	H (MPa)	H (MPa)	H (MPa)	H (MPa)	H (MPa)	H (MPa)
1	1.64	2.07	2.18	1.30	1.95	*2.16*	1.56	1.68	*0.58*
2	1.69	2.59	1.89	1.35	1.69	*2.54*	1.82	1.54	
3	1.58	2.59	1.70	1.30	2.60	*2.48*	1.58	1.50	
4	1.67	2.40	*1.19*	1.43	2.41	*2.54*	1.31	1.52	
5	1.75	2.53	*1.36*	1.36	2.09	*3.27*	1.24	1.67	
6	1.53	2.59	*1.50*	1.34	*1.81*		1.65	1.73	
7	1.80	2.37		1.38	*2.70*		1.42	1.70	
8	1.67			1.73	*3.08*		1.44	2.01	
9	1.84			1.32	*2.67*		1.37	1.94	
10	1.89			1.37	*2.69*		1.44	1.82	
11	1.64			*1.27*			1.28	2.48	
12	1.57			*1.37*			1.28	1.87	
13	1.65			*1.30*			1.59	2.07	
14	1.50			*1.41*			1.63	1.99	
15	1.67			*1.41*			1.21	1.64	
16	1.49			*1.24*					
17	1.65			*1.44*					
18	1.68			*1.47*					
19	1.65			*1.46*					
20	1.63			*1.50*					
average	1.66	2.45	1.64	1.39	2.37	2.60	1.45	1.81	0.58
std dev	0.10	0.18	0.33	0.10	0.43	0.36	0.17	0.25	NA

Note: Italicized values indicate hardness measured at 20 N peak load.

Figure 3.5
Representative load-displacement curves during hardness indentation for AlM in the in-plane and out-of-plane directions.

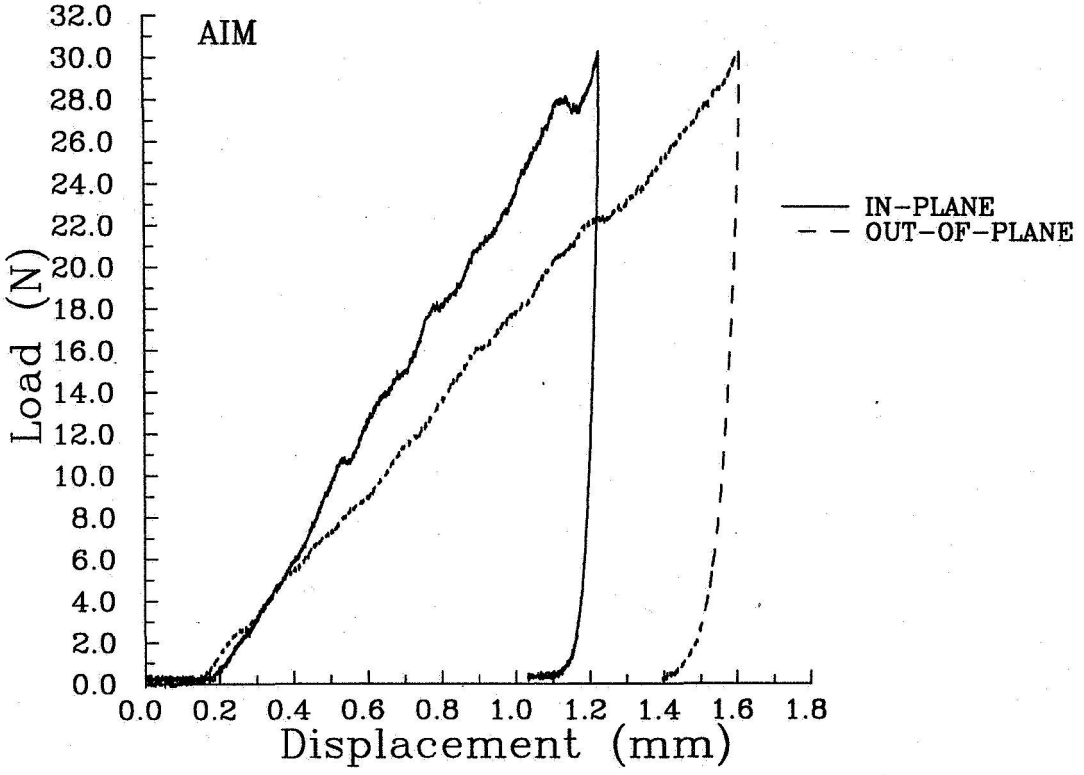

Figure 3.6
Representative load-displacement curves during hardness indentation for FRCI in the in-plane and out-of-plane directions.

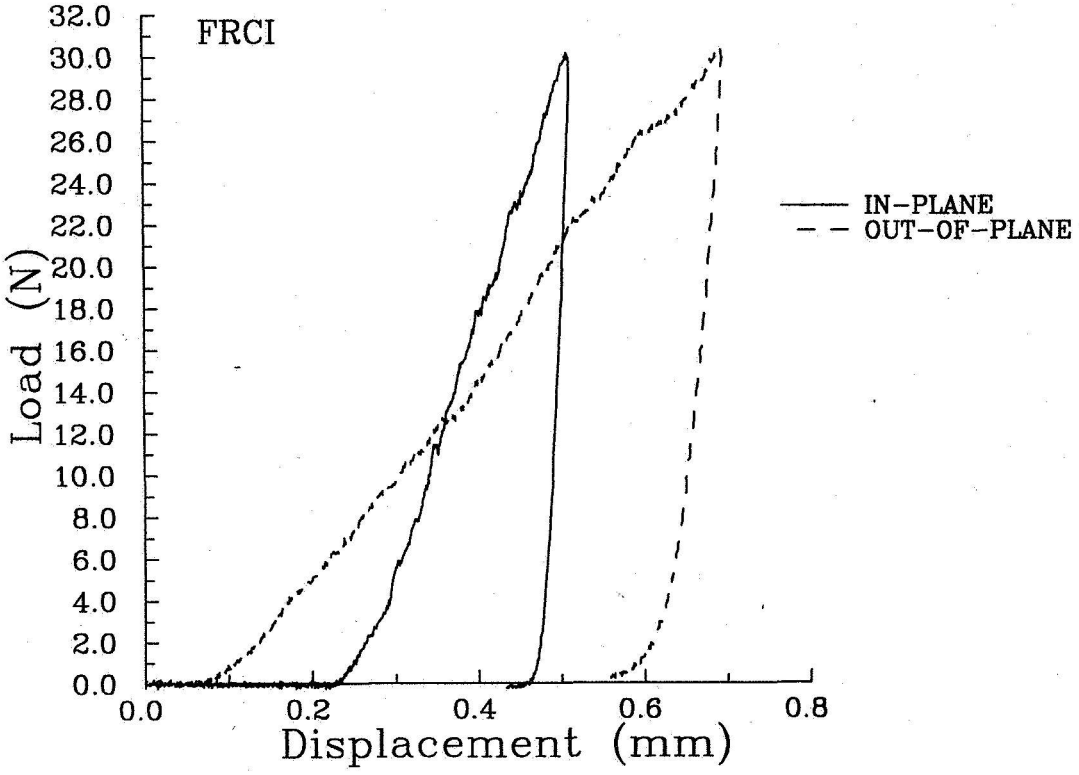

Figure 3.7
Representative load-displacement curves during hardness indentation for Fiberform in the in-plane and out-of-plane directions.

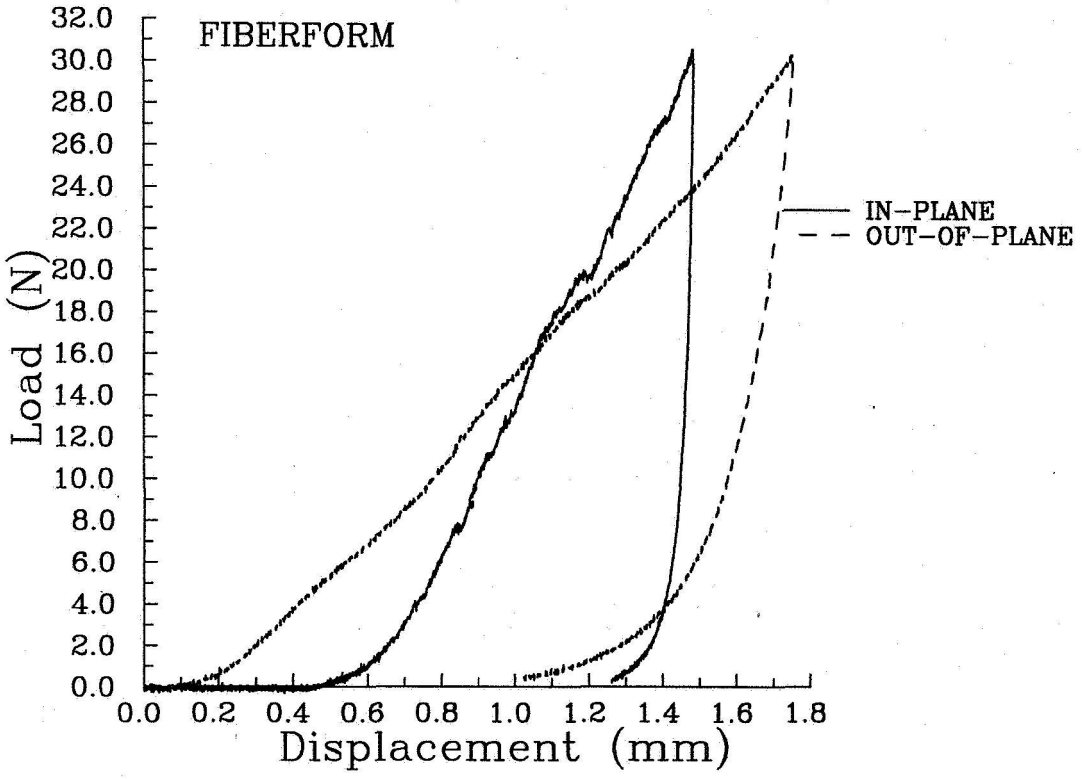

Table 3.2
Hardness values for fibrous substrates in the in-plane and out-of-plane directions.

	AIM		FRCI		Fiberform	
	out-of-plane	in-plane	out-of-plane	in-plane	out-of-plane	in-plane
test #	H (MPa)	H (MPa)	H (Mpa)	H (Mpa)	H (Mpa)	H (Mpa)
1	0.42	0.56	1.20	1.81	0.57	0.72
2	0.44	0.56	1.36	1.89	0.52	0.76
3	0.41	0.53	1.31	1.80	0.53	0.62
4	0.40	0.63	1.30	2.23	0.56	0.60
5	0.40	0.70	1.47	1.95	0.59	0.64
6		0.58		2.27	0.55	0.70
7		0.61		2.11	0.64	0.66
8		0.53		2.46		
9		0.60		2.59		
10		0.61		2.75		
average	0.41	0.59	1.33	2.19	0.57	0.67
std dev	0.01	0.05	0.10	0.33	0.04	0.06

Chapter

4

Compressive Testing

The SIRCA 15A, SIRCA 15F, and PICA materials were subjected to compression tests in their virgin and charred forms. Charring was accomplished by placing the samples in a tube furnace with an argon atmosphere, "ramping" the furnace temperature to 1000°C (at a rate of about 20°C/min), maintaining the temperature at 1000°C for 10 minutes, and cooling to ambient temperature. Compression specimens with 2:1 height:width ratios were cut from virgin and charred materials into rectangular blocks, with nominal dimensions of 0.5" x 0.5" x 1.0". The compression specimens were tested in both the in-plane and out-of-plane directions. The specimens named "in-plane" were cut with the long axis parallel to the fiber orientation and thus the compressive load was applied parallel to the fibers; internal surfaces under pure compression were thus perpendicular to the fibers. Whereas specimens named "out-of-plane" were cut with the long axis perpendicular to the fiber orientation and thus internal surfaces, under compression, were parallel to the fibers. Compression tests were performed with the same displacement-controlled *Instron 1123* testing machine used for hardness tests.

The specimens were placed, one at a time, between the top and bottom portions of a compression fixture, and were loaded by lowering the top portion of the fixture (which was secured to the crosshead). The bottom portion of the compression fixture was a stationary flat plate whereas the top portion consisted of a "frictionless" hemisphere secured into a socket with vacuum grease. The top portion was thus self-aligning. The load was measured with the compression load cell, and the crosshead displacement was measured with the Instron's internal displacement gage. All tests were conducted under ambient conditions. The load-displacement curves were converted to stress-strain curves by dividing the loads by the original cross-sectional areas of the specimens, and the displacements by the original heights of the specimens. Generally, the compression tests were terminated after the maximum load had been reached or when the samples fractured macroscopically. In most cases, macroscopic fracture did not occur. Thus, most experiments were carried out until the load dropped to a point after which recovery to the maximum load would be improbable. In some cases as is discussed below, the stress continued to increase beyond strains of 90%. In these cases, the test was stopped before a maximum stressed was reached.

Examples of in-plane compression tests on virgin LCA materials are shown in Figure 4.1. The characteristic response of each of these materials includes a relatively linear increase of stress with strain, followed by a "topping" or maximum value of stress. The maximum values of stress are typically about 1 to 2 MPa, and they occur at strains of about 0.02 to 0.03. After the maximum stress is reached, the stress strain curves can exhibit a somewhat erratic horizontal path, which is characteristic of internal buckling. In passing we note that similar responses were observed by James and Milstein *[1983]* during compressive failure of single crystals of HgI_2 when loaded in an in-plane manner. (These crystals have a layered atomic structure consisting of atomic planes with strong intraplanar covalent bonding and weak interplanar van der Waals bonding; in-plane loading to the point of fracture causes buckling and separation of the planes.)

By contrast, typical behavior during out of plane compression tests on virgin LCA materials is illustrated schematically in Figure 4.2. In such tests, at stresses less than several tenths of an MPa, and strains under about 0.03, the stress strain response is initially fairly linear and quite repeatable (for a given material). The Young modulus (or ratio of stress to strain) in this region (which is referred to as Ei) ranges from about 10 to 30 MPa. Behavior in this region appears to be a material property, rather then an instrumental or extraneous effect, owing to the fact that it was consistently reproducible. After the initial, relatively linear, response, the slopes of the stress-strain curves drop fairly abruptly and markedly, but then continue to increase, up to strains of about 50% or more, resulting in strongly non-linear, stress-strain responses that have "upward concavities". That is, these materials, under out-of-plane compression, behave somewhat like an accordion, becoming increasingly stiffer as the strain increases.

Among the charred samples that were tested, the behavior of SIRCA 15A (in-plane and out-of-plane), SIRCA 15F (in-plane and out-of-plane), and PICA (in-plane) resembled that shown in Figure 4.1, while charred PICA (out-of-plane) behaved similarly to virgin PICA (out-of-plane), i.e. Figure 4.2. Thus, among the charred materials, only PICA (out-of-plane) exhibited the behavior of Figure 4.2.

Additional examples of stress-strain curves for the samples tested in compression are shown in Figures 4.3 through 4.18. Owing to differences in the characteristic mechanical responses illustrated in Figures 4.1 and 4.2, it is necessary to use different measures to characterize the relevant behaviors. For the specimens that behaved according to Figure 4.1, the compressive strength, the strain at maximum stress, ε_{max}, and two secant moduli, $E_{50\%}$ and $E_{90\%}$, were determined from the stress-strain data. The compressive strength is

defined as the maximum stress carried by the specimens during a test. The strain at which the compressive strength occurs is the strain at maximum stress. Each secant modulus was determined by measuring the slope between two points on the stress-strain curves. For $E_{50\%}$, the slope was calculated between the point of stress equal to 0.05 MPa and the point where the stress is 50% of the compressive strength. For $E_{90\%}$, the slope was calculated between the point of stress equal to 0.05 MPa and the point where the stress is 90% of the compressive strength. The secant moduli indicate the amount of stress required to achieve a given strain, and thus are a measure of the stiffness of the material in the initial "rising" portion of the stress strain curve. The slopes are referenced to the 0.05 MPa value to reduce or eliminate possible effects of surface irregularities.

Among the materials responding as in Figure 4.2, both virgin and charred PICA, tested in the out-of-plane direction, reached maximum values of compressive strength at which failure occurred. Tests of virgin SIRCA 15A and SIRCA 15F in the out-of-plane direction were stopped before the specimens failed (or before a strain of 100% was reached), and hence yielded no maximum compressive strength at which failure occurred. It was unclear for the case of virgin SIRCA 15F that the material would ever fail since strains reached as much as 90%. Thus, for virgin SIRCA 15A and virgin SIRCA 15F, the values of σ_{max} and ε_{max} listed in the tables are the values at which the test was stopped, rather than the values at which "breaking" occurred. Although values of the secant moduli were also determined for specimens that responded as in Figure 4.2, these values are not directly comparable with the values associated with the specimens responding as in Figure 4.1.

The compression results are listed in Tables 4.1 through 4.16. Table 4.1 summarizes the average values of the material parameters mentioned above. Tables 4.2 through 4.15 each represent a different set of tests. In some cases, the same type of material was tested more than once (and the specimens were cut from different batches of material). For example, Tables 4.6 and 4.7 include data from two different sets of experiments with virgin SIRCA 15F, and Tables 4.11 through 4.13 include data from three different sets of experiments with virgin PICA. Table 4.16 compares in-plane hardness values with in-plane compressive strengths. The ratio of compressive strength to hardness ranges from about 0.6 to 0.9.

Among the in-plane tests, materials exhibited higher average compressive strengths after they were subjected to charring, although there is also a greater variation among the charred in-plane data. Charred SIRCA 15F had the overall highest mean compressive

strength (2.67 MPa), followed by charred PICA (1.79 MPa), and then by charred SIRCA 15A (1.51 MPa).

Among materials with a compressive response as in Figure 4.1, a comparison of virgin materials, tested in the in-plane direction, showed that PICA had the largest elastic moduli ($E_{50\%}$ = 143 MPa and $E_{90\%}$ = 106 MPa), followed by SIRCA 15F ($E_{50\%}$ = 130 MPa and $E_{90\%}$ = 126 MPa) and then by SIRCA 15A ($E_{50\%}$ = 80.1 MPa and $E_{90\%}$ = 71.4 MPa). The out-of-plane elastic moduli and maximum stresses of virgin specimens and of charred PICA are not directly comparable to the respective properties measured in the in-plane tests on the virgin materials and on the out-of-plane tests on charred SIRCA, as is discussed above. Hence the former values are not included in Table 4.1. The charring process did not greatly affect the in-plane elastic moduli of SIRCA 15A and PICA. However, the in-plane elastic modulus of the SIRCA 15F increased by about 500% after being charred. This increase in stiffness is the result of both an increase in maximum compressive strength as well as a decrease in strain at the maximum compressive strength. Further testing should be carried out to confirm this immense increase in stiffness.

In order to examine hysteresis in the loading behavior of out-of-plane specimens, eight PICA specimens were successively loaded and unloaded; the stress and strain were monitored during both the loading and unloading cycles, and unloading commenced after various levels of loading. A new specimen was used in each test. That is, each specimen underwent only one load cycle. The results are plotted in Figure 4.19. The area under each stress-strain loop represents the energy dissipated during the particular test. Specimens loaded to similar strains displayed remarkable repeatability. In order to examine the influence of preloading, future tests are planned to see how a single specimen would respond to multiple loading-unloading cycles, as well as to examine the hysteresis in the other LCA materials.

An additional series of tests was run to determine if loading rate affected the compression results. For these tests, the crosshead speed was varied from 0.051 mm/min to 1.016 mm/min. SIRCA 15A in-plane, SIRCA 15F in-plane, and PICA in-plane were tested in this manner. Representative plots of the stress-strain results are provided in Figures 4.20 through 4.22. No significant variations in compression results were observed at different loading rates within the range of rates tested.

If a compression test was allowed to continue until the point of complete macroscopic failure, the area under the stress-strain curve would be indicative of the energy absorption potential of the material. Tests to date indicate that LCAs compressed in the in-plane direction continue to absorb energy at large strains compared with the strain at maximum stress. This is apparent in Figures 4.20 through 4.22 where the stress remains relatively constant from the point of maximum stress (approximately 2% strain) on up to strains of 6% to 9%. The majority of tests to date were not carried beyond this point. Future tests are planned to quantify the total energy absorption of the LCAs up to the point of complete macroscopic failure.

When the charred PICA was subjected to compression testing, the modes of failure correlated directly with the fiber orientation. Figure 4.23 displays the prevailing mode of failure resulting from the out-of-plane fiber orientation. The following are observations captured during testing of charred PICA as represented in Figure 4.23:

- During compression, the material started forming rifts parallel to the fiber orientation. Figure 4.23(a).
- The material failed as a result of 45 degree-angled cracks started on the vertical wall of the sample. Figure 4.23(b). These planes at 45^{o} are planes of maximum shear stress under uniaxial compressive loading.
- A wedged shape piece of the material exploded outward once the two cracks intercepted each other. Figure 4.23(c).

Figure 4.24 displays the prevailing mode of failure resulting from the in-plane fiber orientation of charred PICA. During compression, the material started to form vertical clefts at the top and/or the bottom of the sample. The clefts were also close to the outside surface.

Future work should be directed at correlating mechanical properties with processing variables. For example, Figure 4.14 displays two stress-strain curves that have significantly higher maximum stresses than the other four curves. When the samples were inspected, it was discovered that there was a correlation between density and compressive strength. The specimens with the higher density (214 kg/m^3) had a higher compressive strength (1.5 MPa), while the specimens with the lower density (205.5 kg/m^3) had a lower compressive strength (0.9 MPa). Further testing should be done to establish correlations between processing variables, such as density, and material properties, such as compressive strength, elastic moduli, and hardness.

Table 4.1
Summary of the average values of the maximum compressive stress σmax, the strain ε at σmax, and secant moduli during compression testing of samples with mechanical responses similar to Figure 4.1. "N/A" implies that the characteristic response was as in Figure 4.2, as discussed in the text.

		Virgin		Charred	
Material	Property	In-plane	Out-of-plane	In-plane	Out-of-plane
SIRCA 15A	σ_{max} (MPa)	1.38 ± 0.09	N/A	1.51 ± 0.33	1.20 ± 0.57
	ε @ σ_{max}	0.027 ± 0.003	N/A	0.034 ± 0.007	0.043 ± 0.031
	E(50%) (MPa)	80 ± 8	N/A	88 ± 14	74 ± 23
	E(90%) (MPa)	71 ± 4	N/A	69 ± 25	69 ± 30
SIRCA 15F	σ_{max} (MPa)	*2.08 ± 0.12	N/A	2.67 ± 0.38	2.14 ± 0.92
	ε @ σ_{max}	*0.021 ± 0.001	N/A	0.013 ± 0.01	0.031 ± 0.028
	E(50%) (MPa)	*130 ± 5	N/A	712 ± 106	552 ± 327
	E(90%) (MPa)	*126 ± 5	N/A	534 ± 307	491 ± 308
PICA	σ_{max} (MPa)	*1.55 ± 0.09	N/A	1.79 ± 0.45	N/A
	ε @ σ_{max}	*0.029 ± 0.011	N/A	0.044 ± 0.006	N/A
	E(50%) (MPa)	*143 ± 17	N/A	107 ± 20	N/A
	E(90%) (MPa)	*106 ± 9	N/A	78 ± 23	N/A

* Values are from the first set of experiments with the given material

Table 4.2
Compression results for the virgin SIRCA 15A tested in the in-plane direction.

SIRCA 15A In-Plane									
test #	σmax (MPa)	εmax	ε(0.05)	ε(50%)	ε(90%)	σ(50%) (Mpa)	σ(90%) (Mpa)	E50% (Mpa)	E90% (Mpa)
1	1.33	0.025	0.004	0.012	0.020	0.67	1.20	83	73
2	1.43	0.031	0.004	0.012	0.022	0.71	1.28	78	67
3	1.30	0.025	0.004	0.011	0.020	0.65	1.17	86	73
4	1.41	0.026	0.005	0.013	0.021	0.71	1.27	78	74
5	1.27	0.023	0.004	0.012	0.019	0.63	1.14	80	76
6	1.52	0.033	0.008	0.017	0.027	0.76	1.37	85	71
7	1.44	0.027	0.003	0.011	0.019	0.72	1.30	87	81
8	1.39	0.031	0.006	0.014	0.024	0.70	1.25	86	67
9	1.40	0.026	0.004	0.013	0.022	0.70	1.26	67	66
10	1.21	0.025	0.006	0.013	0.021	0.60	1.09	73	67
11	1.29	0.028	0.006	0.015	0.023	0.65	1.16	67	68
12	1.52	0.029	0.006	0.013	0.024	0.76	1.37	91	73
average	**1.38**	**0.027**						**80**	**71**
std dev	**0.09**	**0.003**						**8**	**4**

Table 4.3

Compression results for the virgin SIRCA 15A tested in the out-of-plane direction. In this table, σ_{max} and ε_{max} do not represent values as failure of the specimens, but rather the values as which the test was stopped, since there was no sign that the specimens were going to fail.

SIRCA 15A Out-of-Plane					
test #	**σmax (MPa)**	**εmax**	**E50% (MPa)**	**E90% (MPa)**	**Ei (MPa)**
1	5.057	0.4753	5.89	9.68	22.70
2	5.484	0.4900	6.12	10.28	23.08
3	5.382	0.4925	5.87	9.99	11.82
4	4.942	0.4708	5.74	9.56	21.32
5	4.981	0.4866	5.53	9.33	17.13
6	5.024	0.4841	5.68	9.48	16.12
7	5.111	0.4877	5.70	9.64	12.16
8	5.072	0.4885	5.64	9.52	16.53
9	5.057	0.4864	5.61	9.47	16.10
average	**5.12**	**0.485**	**5.75**	**9.66**	**17.4**
std. dev	**0.18**	**0.007**	**0.18**	**0.29**	**4.2**

Table 4.4
Compression results for the charred SIRCA 15A tested in the in-plane direction.

Charred SIRCA 15A In-Plane				
test #	**σmax (MPa)**	**εmax**	**E50% (MPa)**	**E90% (MPa)**
1	0.901	0.0415	67.42	34.22
2	1.057	0.0192	73.8	68.1
3	1.405	0.0350	84.4	55.3
4	1.991	0.0385	113	122.0
5	1.906	0.0431	86.94	56.44
6	1.179	0.0296	110.29	45.22
7	1.733	0.0405	78.98	56.60
8	1.516	0.0343	91.37	61.85
9	1.514	0.0322	79.77	70.11
10	1.614	0.0325	75.44	72.95
11	1.571	0.0381	86.75	55.72
12	1.326	0.0253	84.98	77.72
13	1.872	0.0273	110.75	117.06
average	**1.51**	**0.0336**	**88.0**	**68.7**
Std dev	**0.33**	**0.0069**	**14.7**	**25.4**

Table 4.5
Compression results for the charred SIRCA 15A tested in the out-of-plane direction.

Charred SIRCA 15A Out-of-Plane				
test #	σmax (MPa)	εmax	E50% (MPa)	E90% (MPa)
1	2.134	0.0259	102.0	101.0
2	0.799	0.0646	48.5	25.4
3	0.831	0.0564	59.8	51.9
4	0.971	0.0557	53.38	47.3
5	0.963	0.0470	58.68	44.1
6	0.784	0.1264	65.71	65.7
7	0.913	0.0365	68.1	62.3
8	0.893	0.0187	66.6	66.4
9	1.814	0.0255	113.0	121.0
10	0.893	0.0177	62.9	58.8
11	2.401	0.0235	118.0	122.0
12	1.046	0.0195	69.65	64.68
average	**1.20**	**0.0431**	**73.9**	**69.2**
std dev	**0.57**	**0.0310**	**23.5**	**30.2**

Table 4.6
Compression results for the virgin SIRCA 15F tested in the in-plane direction.
(Note the different values measured in tests #1-8 compared with tests #9-12.)

SIRCA 15F In-Plane									
test #	σmax (MPa)	εmax	ε(0.05)	ε(50%)	ε(90%)	σ(50%) (Mpa)	σ(90%) (Mpa)	E50% (Mpa)	E90% (Mpa)
1	1.968	0.0207	0.0044	0.0118	0.0184	0.984	1.771	126.2	122.9
2	2.334	0.0231	0.0054	0.0140	0.0209	1.167	2.101	129.9	132.3
3	2.028	0.0205	0.0035	0.0107	0.0175	1.014	1.825	133.9	126.8
4	2.097	0.0201	0.0039	0.0116	0.0185	1.049	1.887	129.7	125.8
5	1.978	0.0217	0.0043	0.0114	0.0183	0.989	1.780	132.3	123.6
6	1.996	0.0211	0.0039	0.0118	0.0188	0.998	1.796	120.0	117.2
7	2.190	0.0196	0.0033	0.0108	0.0176	1.095	1.971	139.3	134.3
8	2.015	0.0222	0.0046	0.0121	0.0191	1.008	1.814	127.7	121.7
average	**2.08**	**0.0211**						**130**	**126**
std dev	**0.12**	**0.0011**						**5**	**5**
9	1.536	0.0250	0.0077	0.0159	0.0225	0.768	1.382	87.6	90.0
10	1.612	0.0276	0.0086	0.0159	0.0223	0.806	1.451	103.6	102.3
11	1.667	0.0210	0.0033	0.0107	0.0171	0.834	1.500	105.9	105.1
12	1.729	0.0205	0.0039	0.0114	0.0181	0.865	1.556	108.7	106.1
average	**1.64**	**0.0235**						**101**	**101**
std dev	**0.07**	**0.0029**						**8**	**6**

Table 4.7
Compression results for the virgin SIRCA 15F tested in the in-plane direction.

SIRCA 15F In-Plane				
test #	**σmax (MPa)**	**εmax**	**E50% (MPa)**	**E90% (MPa)**
1a	1.139	0.0207	69.1	47.9
2a	1.378	0.0228	79.9	49.7
3a	1.394	0.0204	83.2	83.2
4a	0.982	0.0356	66.7	66.2
5a	2.343	0.0274	110.9	115.5
6a	1.416	0.0002	98.5	100.2
average	**1.44**	**0.0212**	**84.7**	**77.1**
std dev	**0.47**	**0.0118**	**17.1**	**27.5**

Table 4.8
Compression results for virgin SIRCA 15F tested in the out-of-plane direction. During these tests, maximum stresses, σ_{max}, of 6 – 13 MPa and corresponding strains, ε_{max}, of up to 90% were reached without failure of the specimens.

SIRCA 15F Out-of-plane				
test #	Ei(50%) (MPa)	Ei(90%) (MPa)	E50% (MPa)	E90% (MPa)
1	29.7	26.3	3.7	6.2
2	27.2	20.9	7.6	13.3
3	31.7	28.7	2.4	3.8
4	23.8	21.4	7.0	12.0
5	34.2	29.7	4.5	7.7
6	31.8	27.4	4.6	8.0
7	19.4	19.4	4.8	8.2
8	35.7	32.6	4.4	7.5
9	36.5	31.6	3.8	6.6
10	32.3	26.8	7.8	13.7
average	**30.2**	**26.5**	**5.1**	**8.7**
std. dev	**5.4**	**4.6**	**1.8**	**3.2**

Table 4.9
Compression results for the charred SIRCA 15F tested in the in-plane direction.

Charred SIRCA 15F In-Plane				
test #	σmax (MPa)	εmax	E50% (MPa)	E90% (MPa)
1	2.982	0.0150	829.6	791.8
2	2.989	0.0317	736.7	138.1
3	2.167	0.0062	652.5	614.8
4	2.355	0.0053	614.1	647.1
5	2.711	0.0050	699.5	757.2
6	2.272	0.0059	634.0	599.1
7	3.337	0.0048	930.6	994.6
8	2.339	0.0061	602.9	546.7
9	2.596	0.0270	769.8	104.0
10	2.911	0.0268	647.5	142.8
Average	**2.67**	**0.0134**	**712**	**534**
Std. Dev.	**0.38**	**0.0109**	**106**	**307**

Table 4.10
Compression results for the charred SIRCA 15F tested in the out-of-plane direction.

Charred SIRCA 15F Out-of-Plane				
test #	σmax (MPa)	εmax	E50% (MPa)	E90% (MPa)
1	2.994	0.0123	277.8	278.4
2	1.022	0.0520	202.6	223.8
3	2.698	0.0346	581.2	661.5
4	1.278	0.0649	272.0	210.3
5	3.672	0.0041	951.9	966.0
6	2.534	0.0046	652.8	642.4
7	2.530	0.0050	905.6	816.3
8	1.198	0.0613	264.8	175.4
9	2.341	0.0035	1068.4	764.7
10	1.166	0.0685	342.1	174.1
Average	**2.14**	**0.0311**	**552**	**491**
Std. Dev	**0.92**	**0.0281**	**327**	**308**

Table 4.11
Compression results for PICA tested in the in-plane and out-of-plane directions.

PICA In-Plane									
test #	σmax (MPa)	εmax	ε(0.05)	ε(50%)	ε(90%)	σ(50%) (MPa)	σ(90%) (MPa)	E50% (MPa)	E90% (MPa)
1	1.530	0.0298	0.0068	0.0127	0.0222	0.765	1.377	121.2	86.2
2	1.445	0.0252	0.0060	0.0113	0.0194	0.723	1.301	127.0	93.4
3	1.746	0.0240	0.0057	0.0105	0.0189	0.873	1.571	171.5	115.2
4	1.584	0.0613	0.0041	0.0091	0.0167	0.792	1.426	148.4	109.2
5	1.444	0.0232	0.0045	0.0096	0.0168	0.722	1.300	131.8	101.6
6	1.563	0.0421	0.0039	0.0094	0.0169	0.782	1.407	133.1	104.4
7	1.611	0.0387	0.0065	0.0116	0.0198	0.806	1.450	148.2	105.3
8	1.613	0.0247	0.0040	0.0091	0.0166	0.807	1.452	148.4	111.3
9	1.566	0.0238	0.0067	0.0116	0.0193	0.783	1.409	149.6	107.9
10	1.591	0.0406	0.0034	0.0082	0.0165	0.796	1.432	155.4	105.5
11	1.630	0.0224	0.0048	0.0096	0.0176	0.815	1.467	159.4	110.7
12	1.476	0.0206	0.0041	0.0091	0.0164	0.738	1.328	137.6	103.9
13	1.599	0.0206	0.0035	0.0086	0.0161	0.800	1.439	147.1	110.2
14	1.652	0.0185	0.0035	0.0082	0.0153	0.826	1.487	165.1	121.8
15	1.438	0.0212	0.0072	0.0118	0.0184	0.719	1.294	145.4	111.1
16	1.574	0.0296	0.0061	0.0108	0.0189	0.787	1.417	156.8	106.8
17	1.358	0.0256	0.0094	0.0158	0.0227	0.679	1.222	98.3	88.1
18	1.531	0.0207	0.0058	0.0111	0.0180	0.766	1.378	135.1	108.9
average	**1.55**	**0.0285**						**143**	**106**
std dev	**0.09**	**0.0105**						**17**	**9**
PICA Out-of-Plane									
test #	**σmax**	**εmax**	**ε(0.05)**	**ε(50%)**	**ε(90%)**	**σ(50%)**	**σ(90%)**	**E50%**	**E90%**
1	6.096	0.6820	0.0060	0.5490	0.6520	3.048	5.486	5.5	8.4
2	6.179	0.7050	0.0073	0.5880	0.6870	3.090	5.561	5.2	8.1
3	6.345	0.6990	0.0069	0.5650	0.6720	3.173	5.711	5.6	8.5
4	7.011	0.7260	0.0097	0.6020	0.7020	3.506	6.310	5.8	9.0
average	**6.41**	**0.7030**						**5.5**	**8.5**

Table 4.12
Compression results for PICA tested in the in-plane directions.

PICA In-Plane test #	σmax (MPa)	εmax	E50% (MPa)	E90% (MPa)
13a	1.618	0.0255	76.8	75.2
14a	0.968	0.0264	65.6	55.6
15a	0.976	0.0307	54.1	53.4
16a	0.935	0.0282	59.3	55.0
17a	1.524	0.0271	85.2	78.0
18a	0.917	0.0241	67.6	57.7
Average	**1.16**	**0.0270**	**68.1**	**62.5**
Std Dev	**0.32**	**0.0023**	**11.4**	**11.0**

Table 4.13
Compression results for PICA tested in the out-of-plane directions.

PICA Out-of-Plane test #	σmax (MPa)	εmax	E50% (MPa)	E90% (MPa)
1a	4.921	0.7290	4.4	6.7
2a	5.182	0.7176	4.5	7.0
3a	4.390	0.6859	3.9	6.0
4a	4.990	0.7132	4.5	6.6
5a	5.211	0.7336	4.5	6.8
6a	5.015	0.7293	4.3	6.5
7a	4.848	0.7100	4.3	6.5
Average	**4.94**	**0.717**	**4.3**	**6.6**
Std. Dev	**0.27**	**0.016**	**0.2**	**0.3**

Table 4.14
Compression results for the charred PICA tested in the in-plane directions.

Charred PICA In-Plane				
test #	σmax (MPa)	εmax	E50% (MPa)	E90% (MPa)
1	2.864	0.03410	149.61	128.57
2	1.571	0.04586	87.90	63.05
3	1.889	0.05238	111.53	82.74
4	1.547	0.04719	96.28	61.79
5	1.700	0.03760	95.00	73.01
6	1.417	0.04045	92.17	63.53
7	1.635	0.04921	101.70	69.72
8	2.303	0.04968	130.96	108.23
9	1.524	0.04576	101.87	67.20
10	1.287	0.03538	87.87	52.78
11	1.966	0.04452	120.65	84.12
Average	**1.79**	**0.0438**	**107**	**78**
Std. Dev.	**0.45**	**0.0061**	**20**	**23**

Table 4.15
Compression results for the charred PICA tested in the out-of-plane directions.

Charred PICA Out-of-Plane					
test #	σmax (MPa)	εmax	Ei (MPa)	E50% (MPa)	E90% (MPa)
1	2.508	0.593	14.93	3.06	4.00
2	4.101	0.734	23.75	3.48	5.15
3	2.631	0.679	19.17	2.68	3.65
4	4.071	0.722	28.99	3.57	5.16
5	3.581	0.711	22.22	3.53	4.77
6	4.221	0.694	21.14	4.02	5.74
7	3.174	0.716	13.53	2.99	4.45
8	4.067	0.728	17.98	3.53	5.24
Average	**3.54**	**0.697**	**20.20**	**3.36**	**4.77**
Std. Dev	**0.69**	**0.046**	**4.97**	**0.42**	**0.70**

Table 4.16
Comparison of Hardness and Compressive Strength for LCAs

Material	Hardness (Mpa)	Compressive Strength (MPa)	Ratio of Compressive Strength to Hardness
SIRCA 15A in-plane	2.45	1.38	0.56
SIRCA 15A charred in-plane	1.64	1.507	0.91
SIRCA 15F in-plane	2.37	2.08	0.88
PICA in-plane	1.81	1.55	0.86

Figure 4.1
Representative stress-strain curves during in-plane compression testing of each type of virgin material.

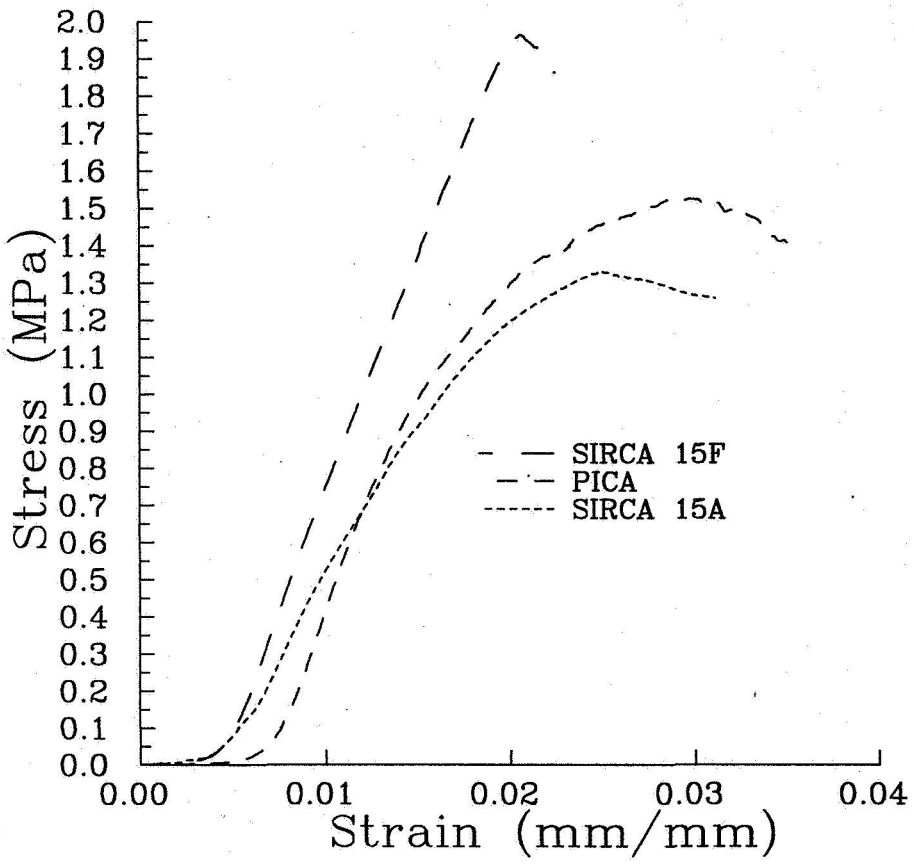

Figure 4.2
Schematic of a stress-strain curve during out-of-plane compression testing of a virgin material.

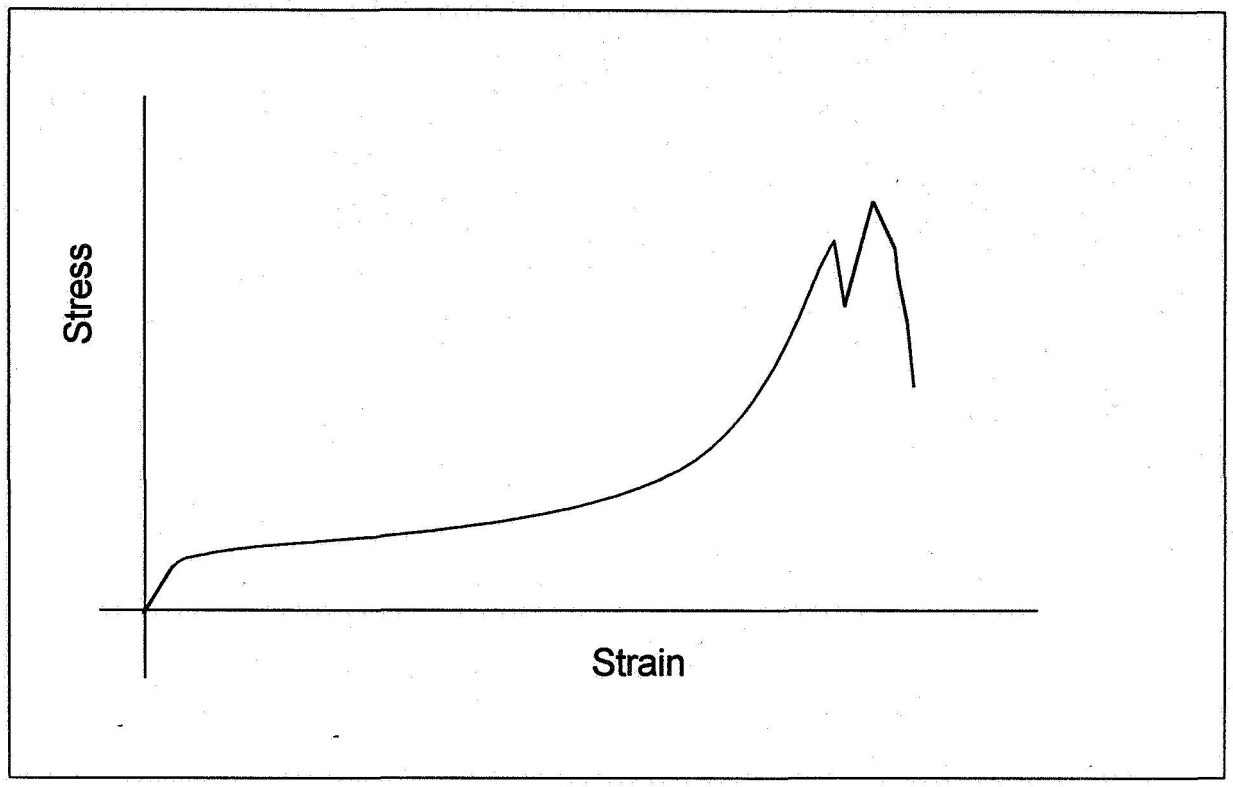

Figure 4.3
Representative stress-strain curves during compression testing of SIRCA 15A in the in-plane direction. Tests #1-10 are shown.

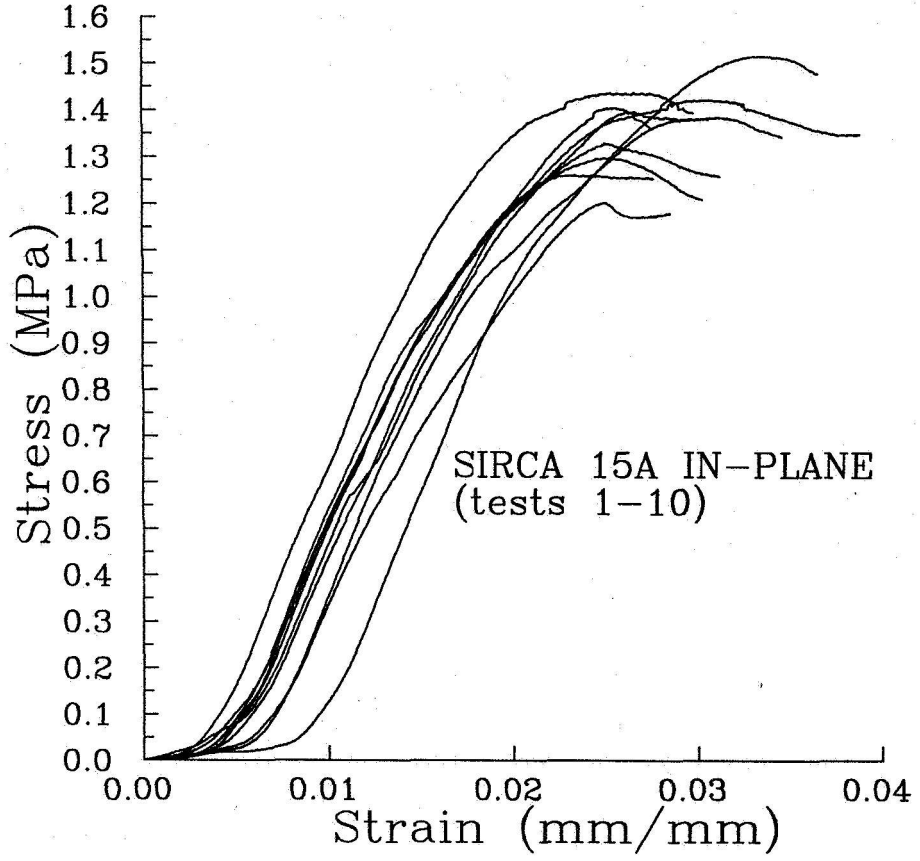

Figure 4.4
Representative stress-strain curves during compression testing of SIRCA 15A in the out-of-plane direction. Tests #1-9 are shown.

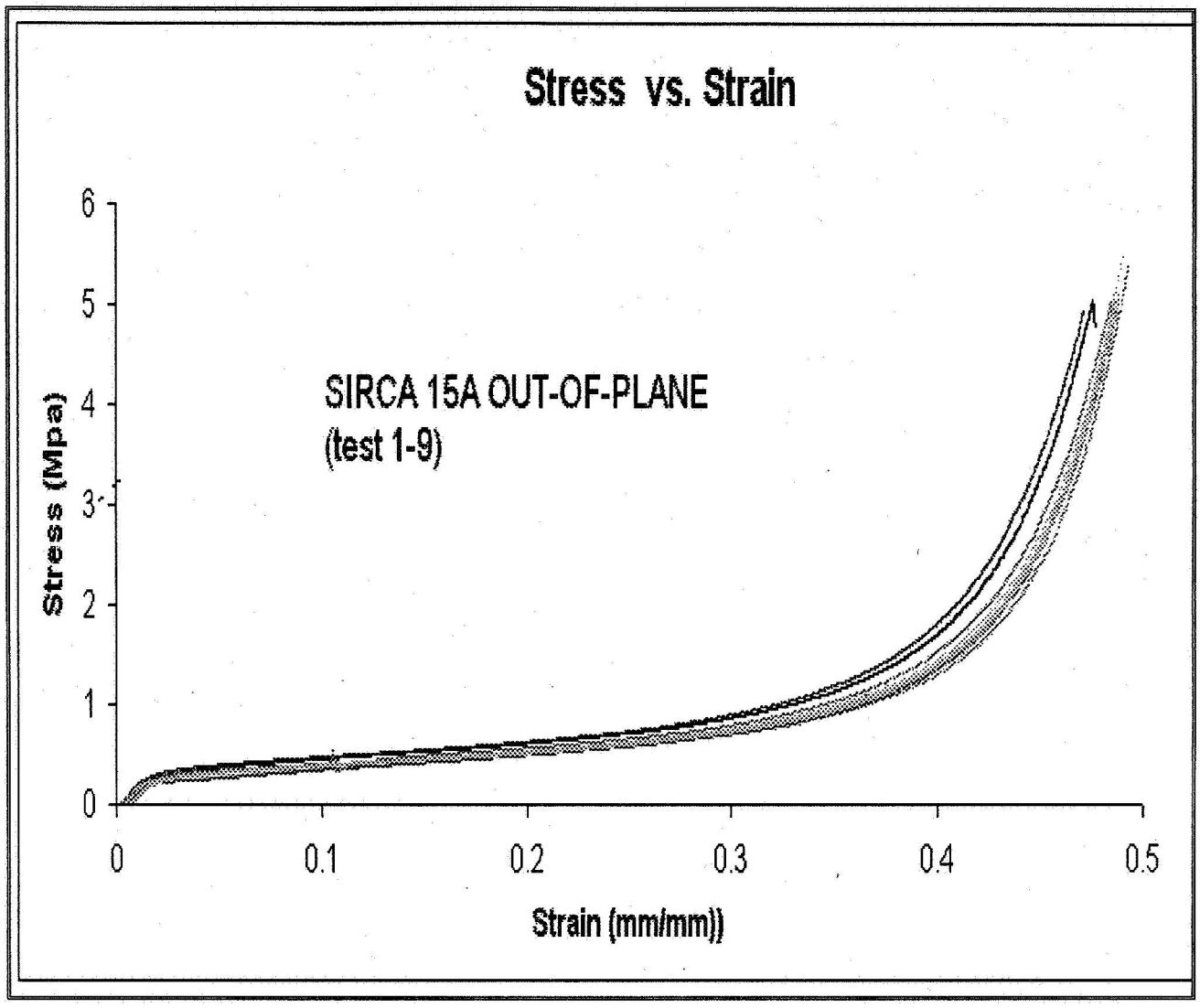

Figure 4.5
Representative stress-strain curves during compression testing of charred SIRCA 15A in the in-plane direction. Tests #1-13 are shown.

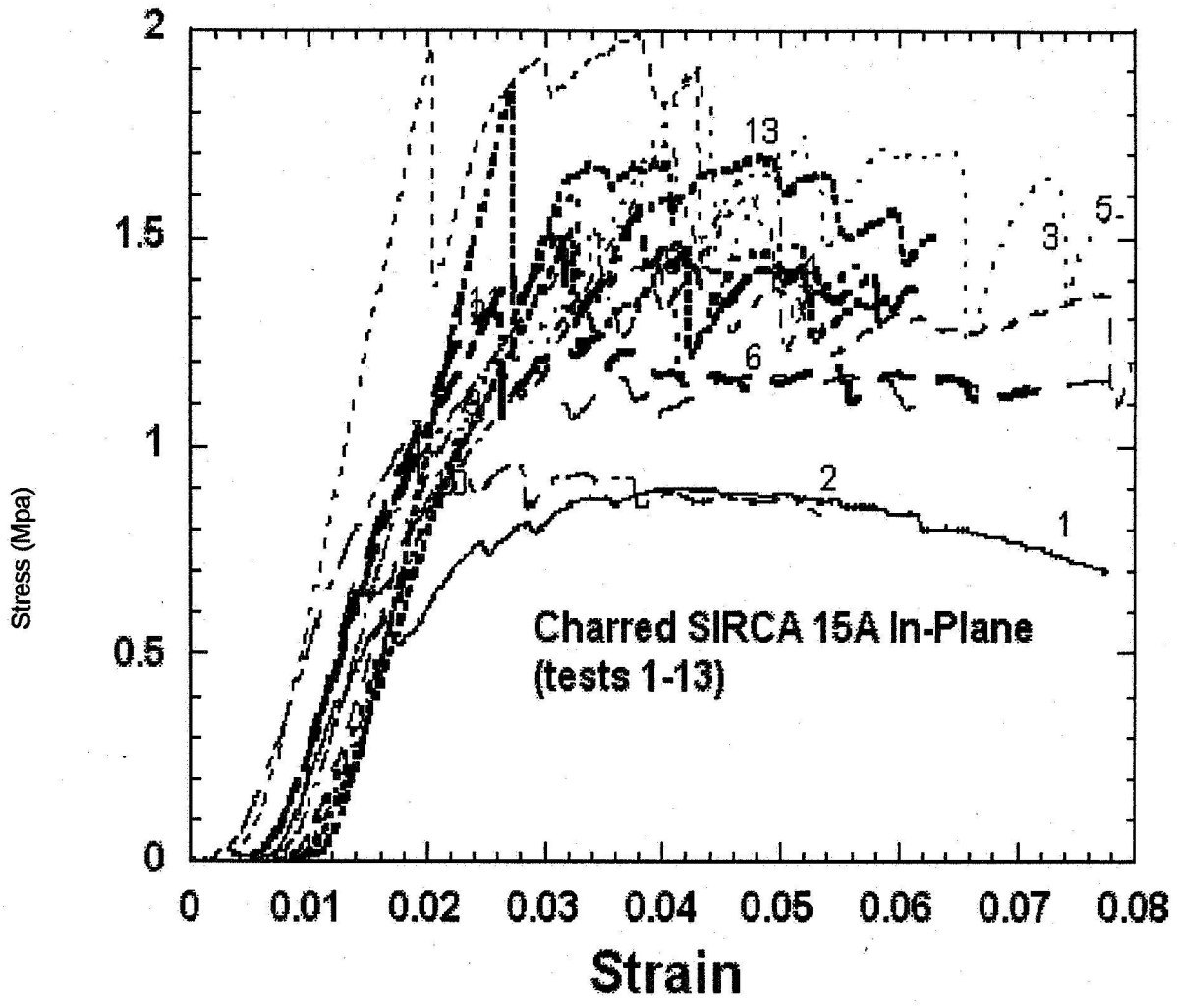

Figure 4.6
Representative stress-strain curves during compression testing of charred SIRCA 15A in the out-of-plane direction. Tests #1-12 are shown.

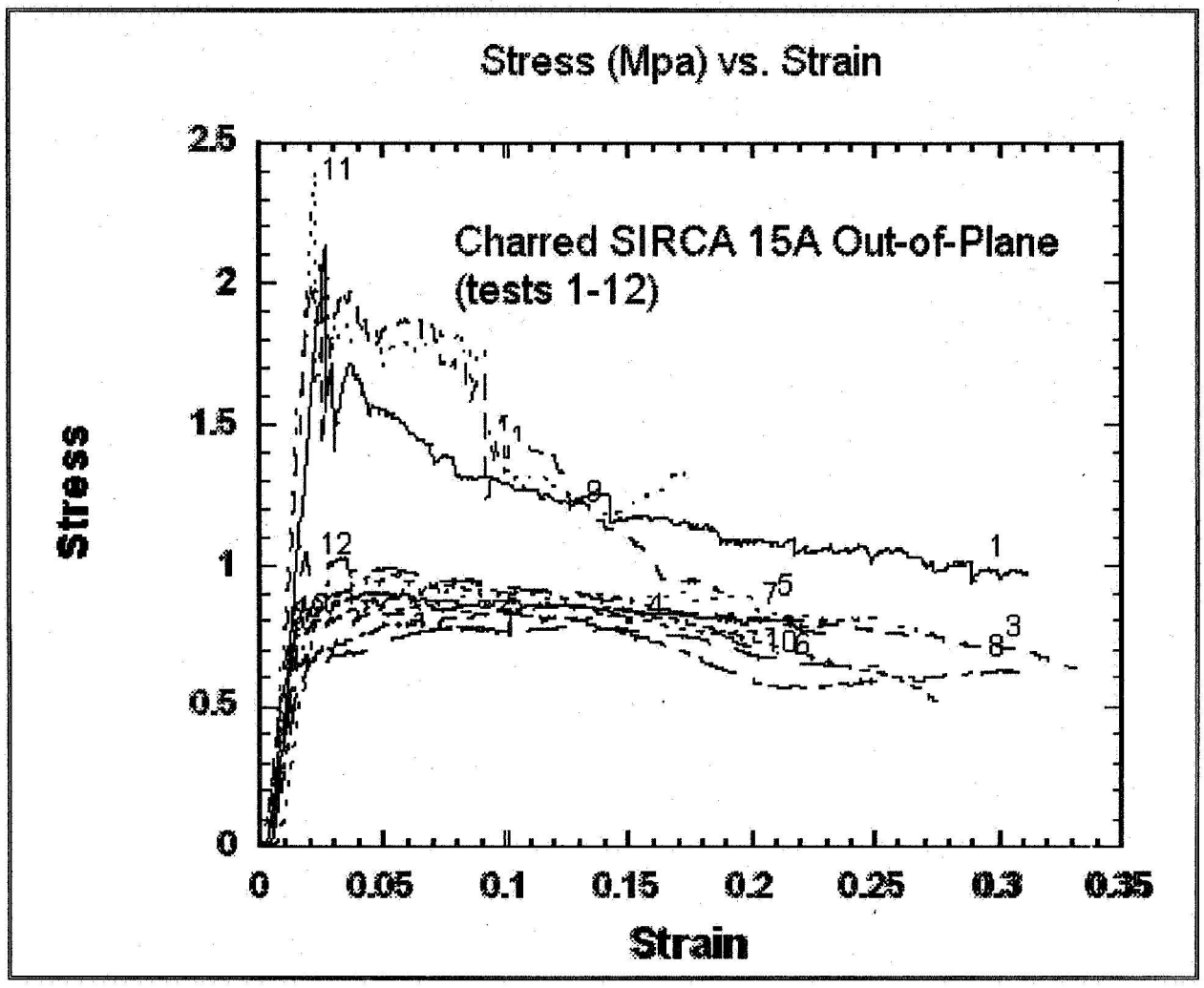

Figure 4.7
Representative stress-strain curves during compression testing of SIRCA 15F in the in-plane direction. Tests #1-8 are shown.

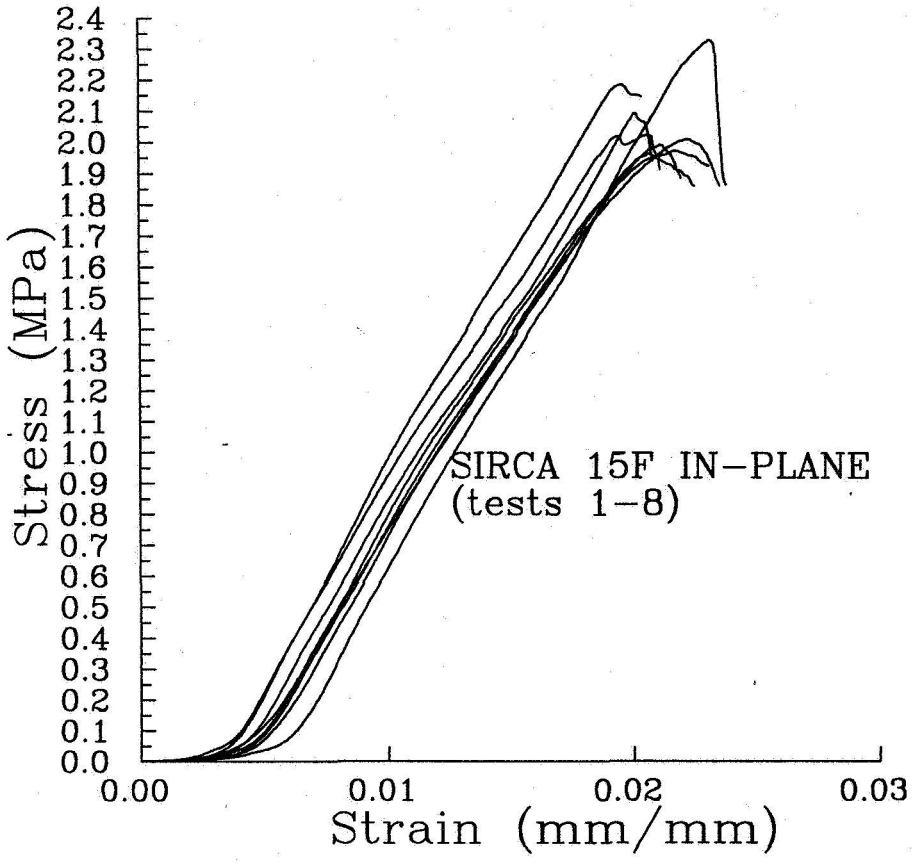

Figure 4.8
Representative stress-strain curves during compression testing of SIRCA 15F in the in-plane direction. Tests #9-12 are shown.

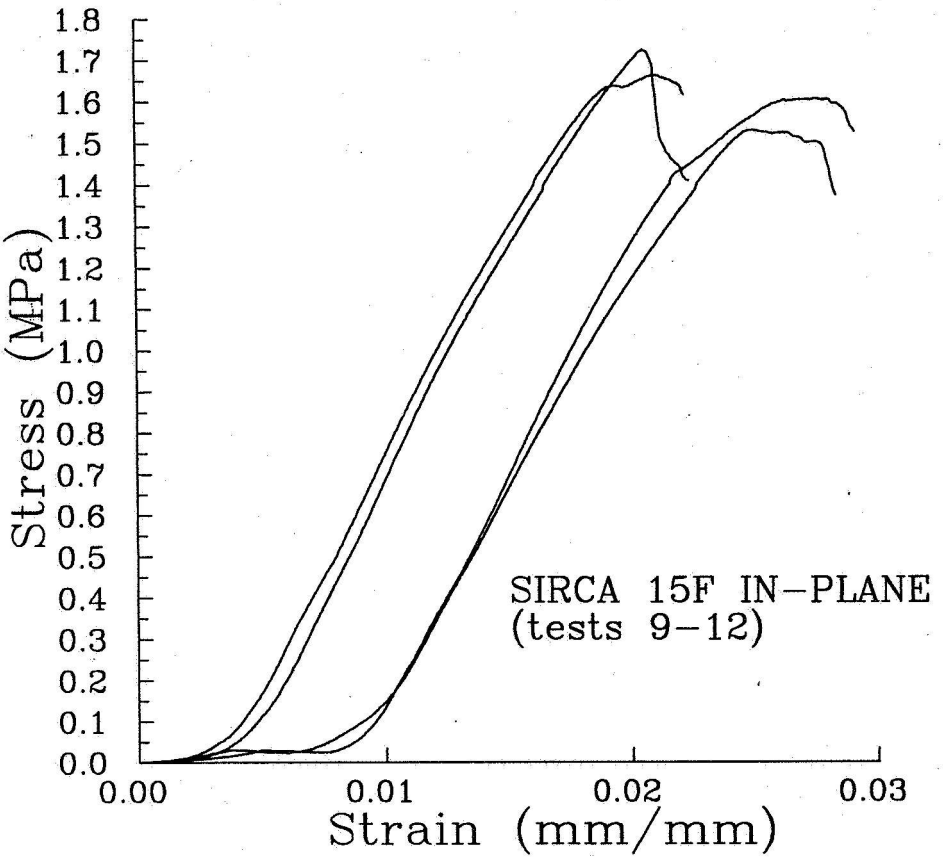

Figure 4.9
Representative stress-strain curves during compression testing of SIRCA 15F in the in-plane direction. Tests #1a-6a are shown.

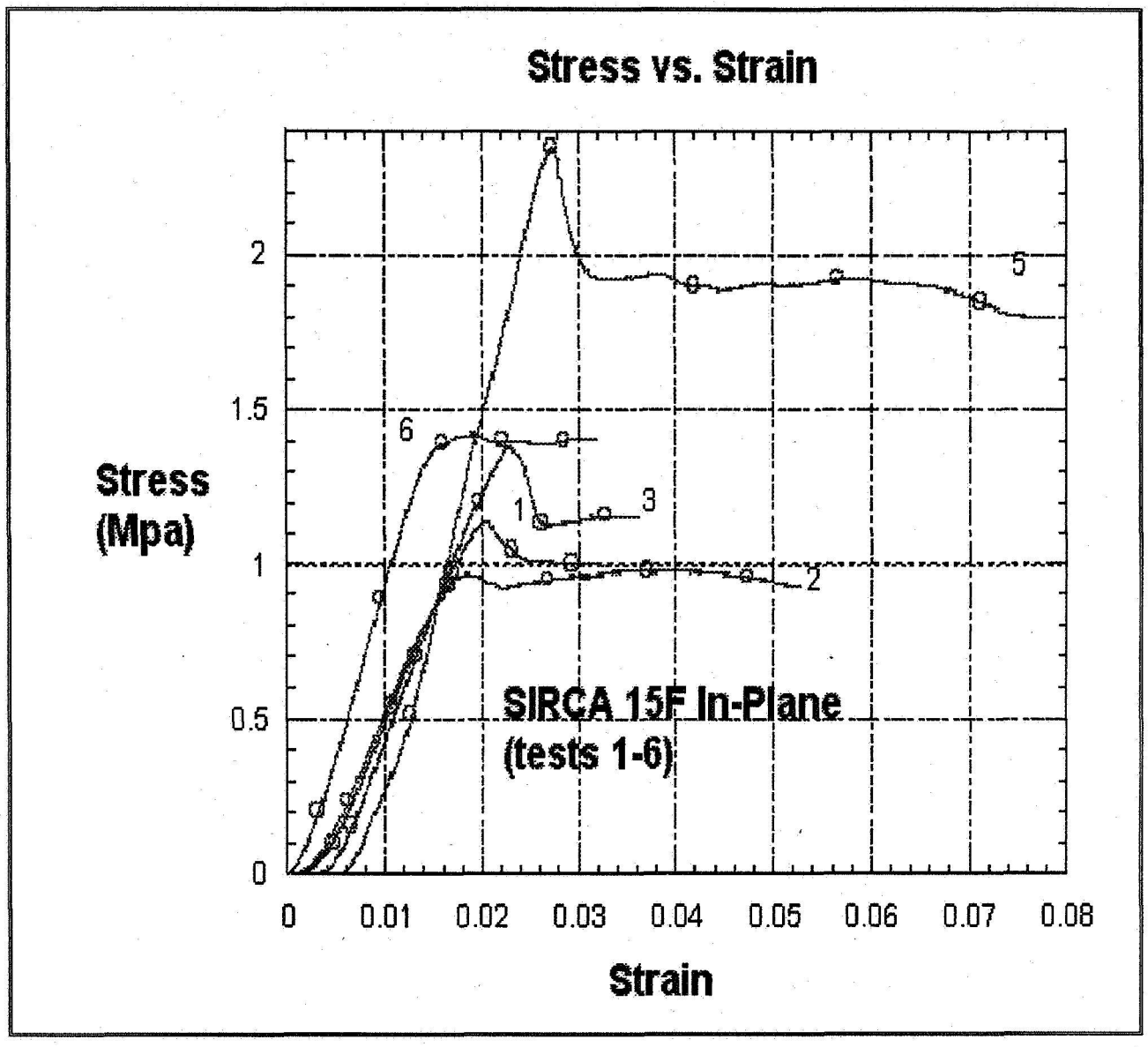

Figure 4.10
Representative stress-strain curves during compression testing of SIRCA 15F in the out-of-plane direction. Tests #1-10 are shown.

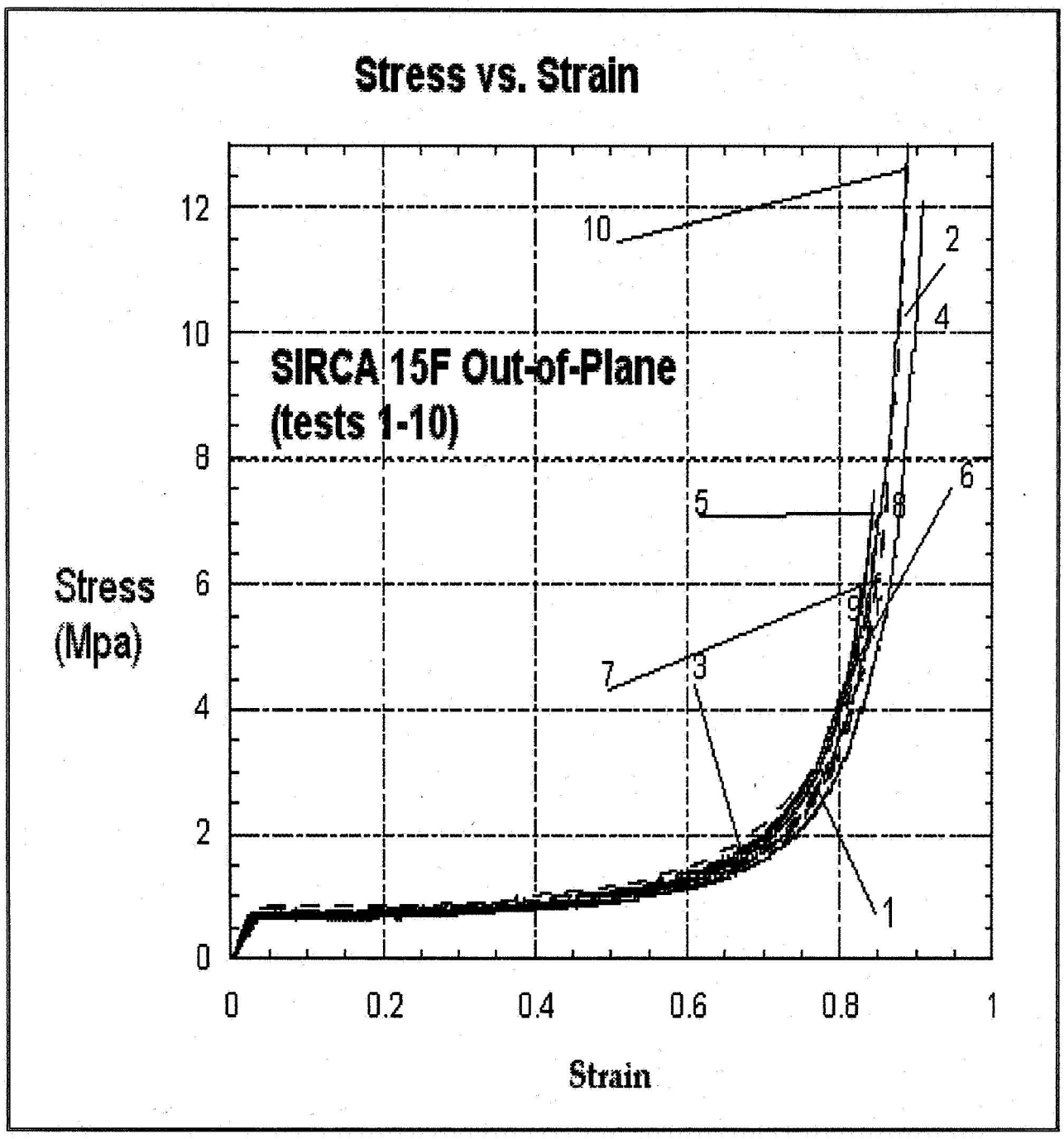

Figure 4.11
Representative stress-strain curves during compression testing of charred SIRCA 15F in the in-plane direction. Tests #1-9 are shown.

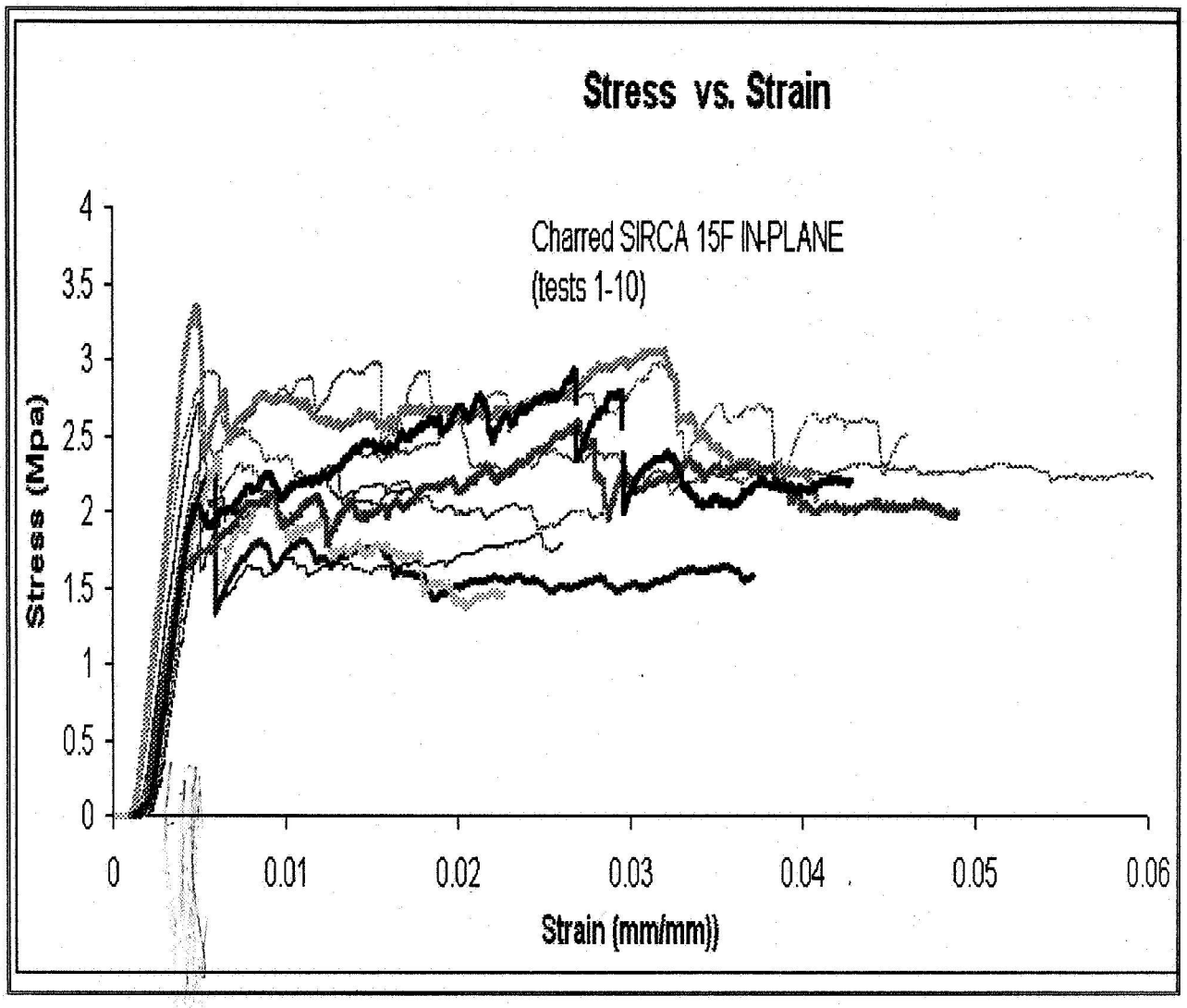

0.03

Figure 4.12
Representative stress-strain curves during compression testing of charred SIRCA 15F in the out-of-plane direction. Tests #1-10 are shown.

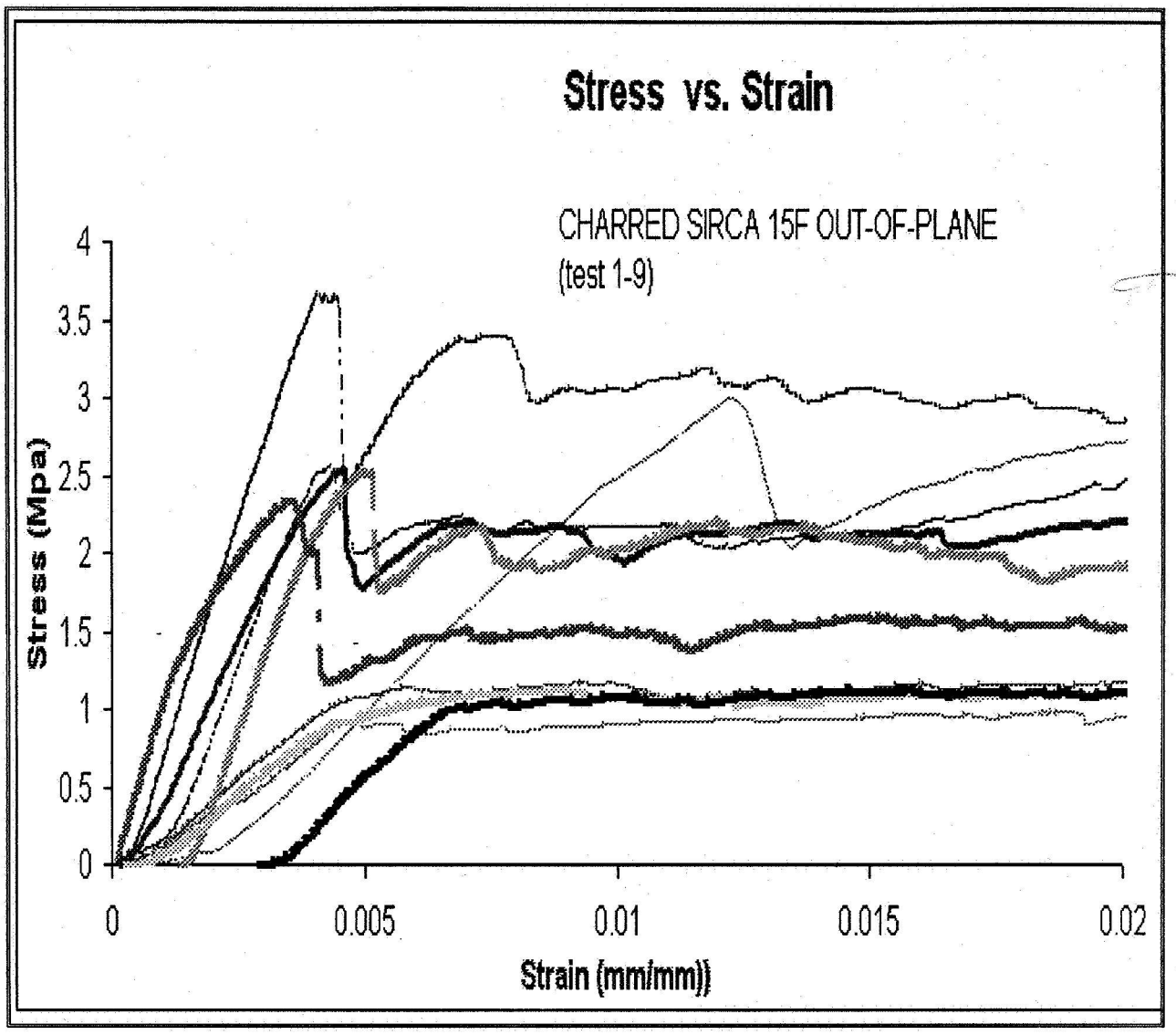

Figure 4.13
Representative stress-strain curves during compression testing of PICA in the in-plane direction. Tests #1-10 are shown.

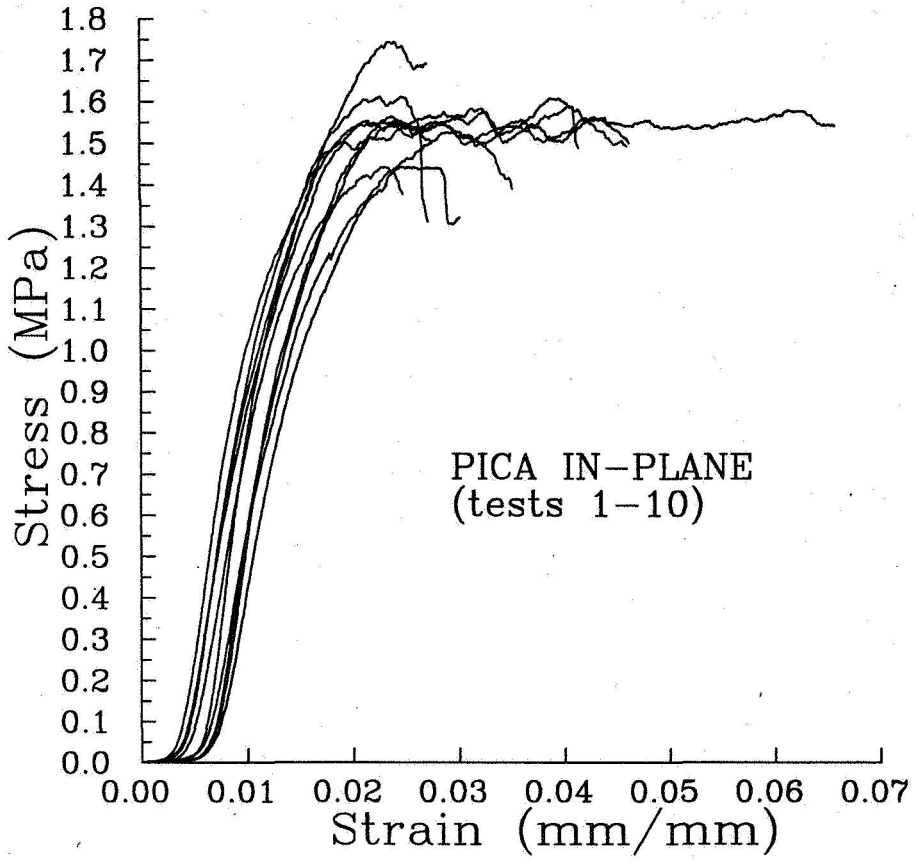

Figure 4.14
Representative stress-strain curves during compression testing of PICA in the in-plane direction. Tests #13a-18a are shown.

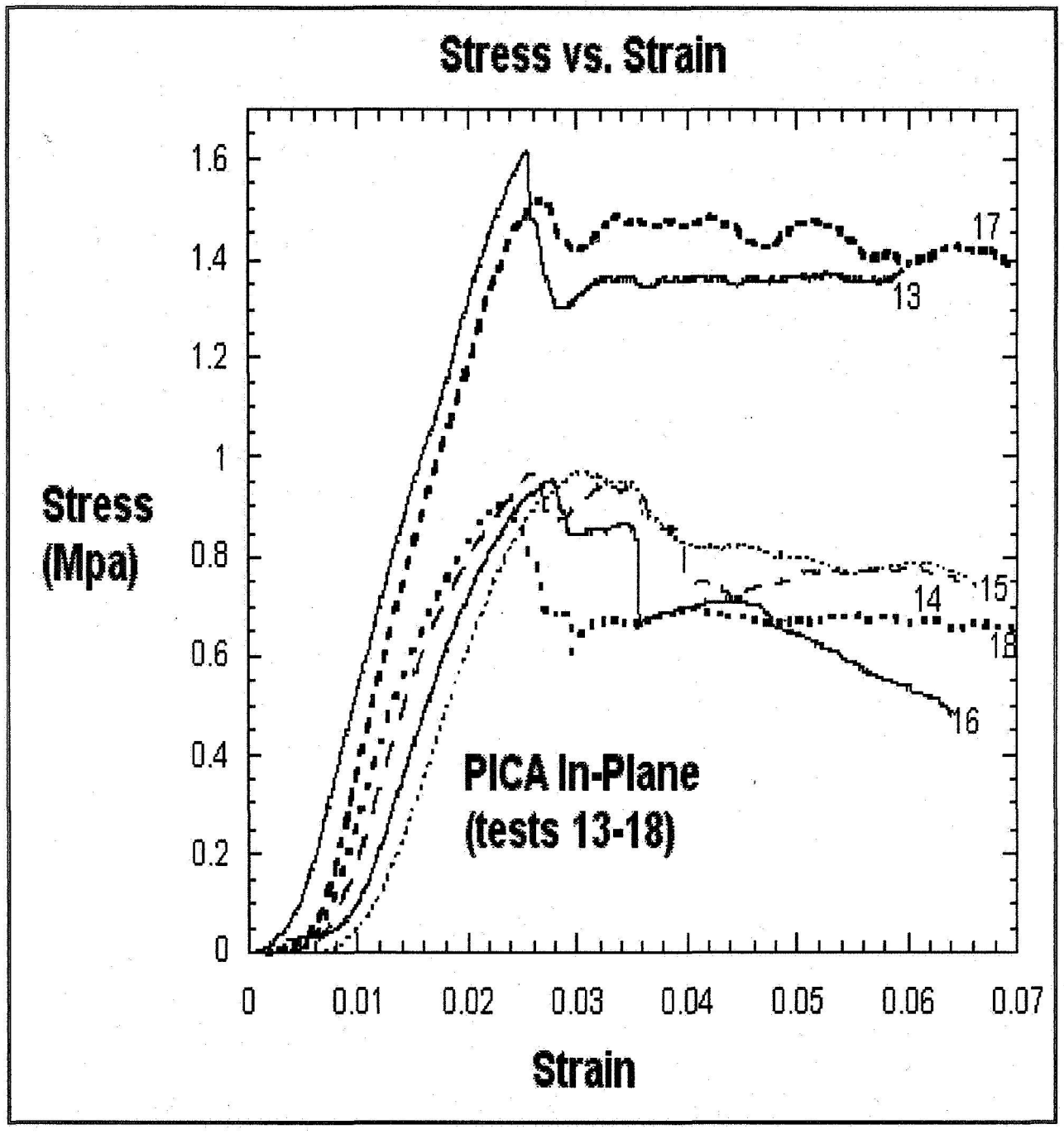

Figure 4.15
Representative stress-strain curves during compression testing of PICA in the out-of-plane direction. Tests #1-4 are shown.

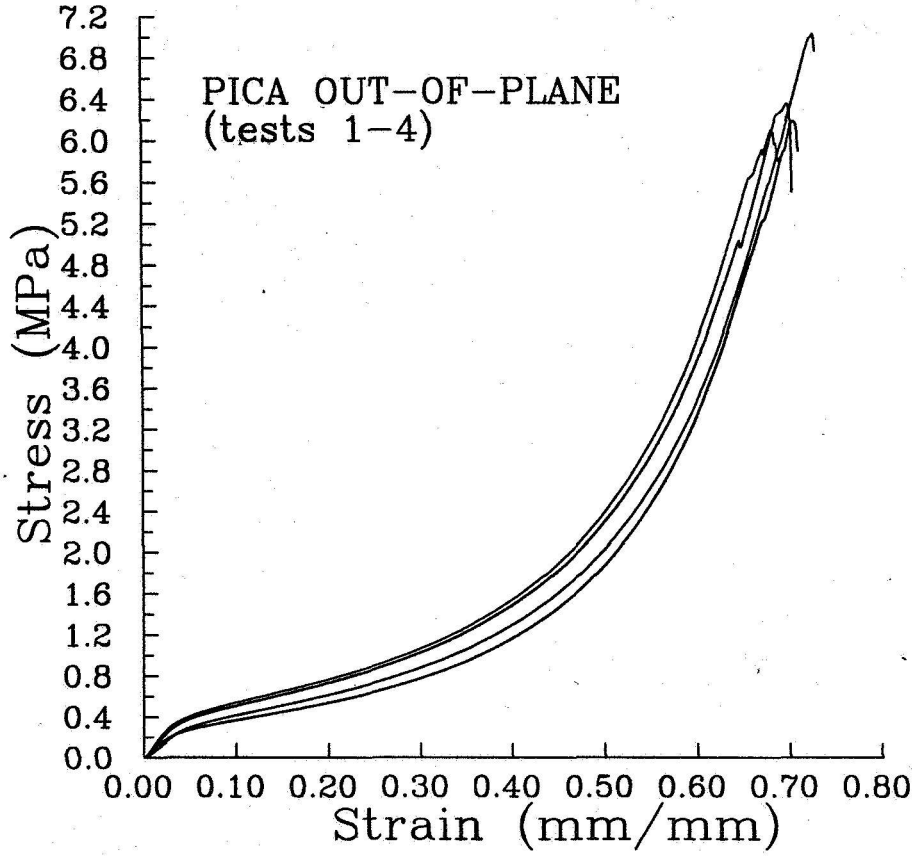

Figure 4.16
Representative stress-strain curves during compression testing of PICA in the out-of-plane direction. Tests #1a-6a are shown.

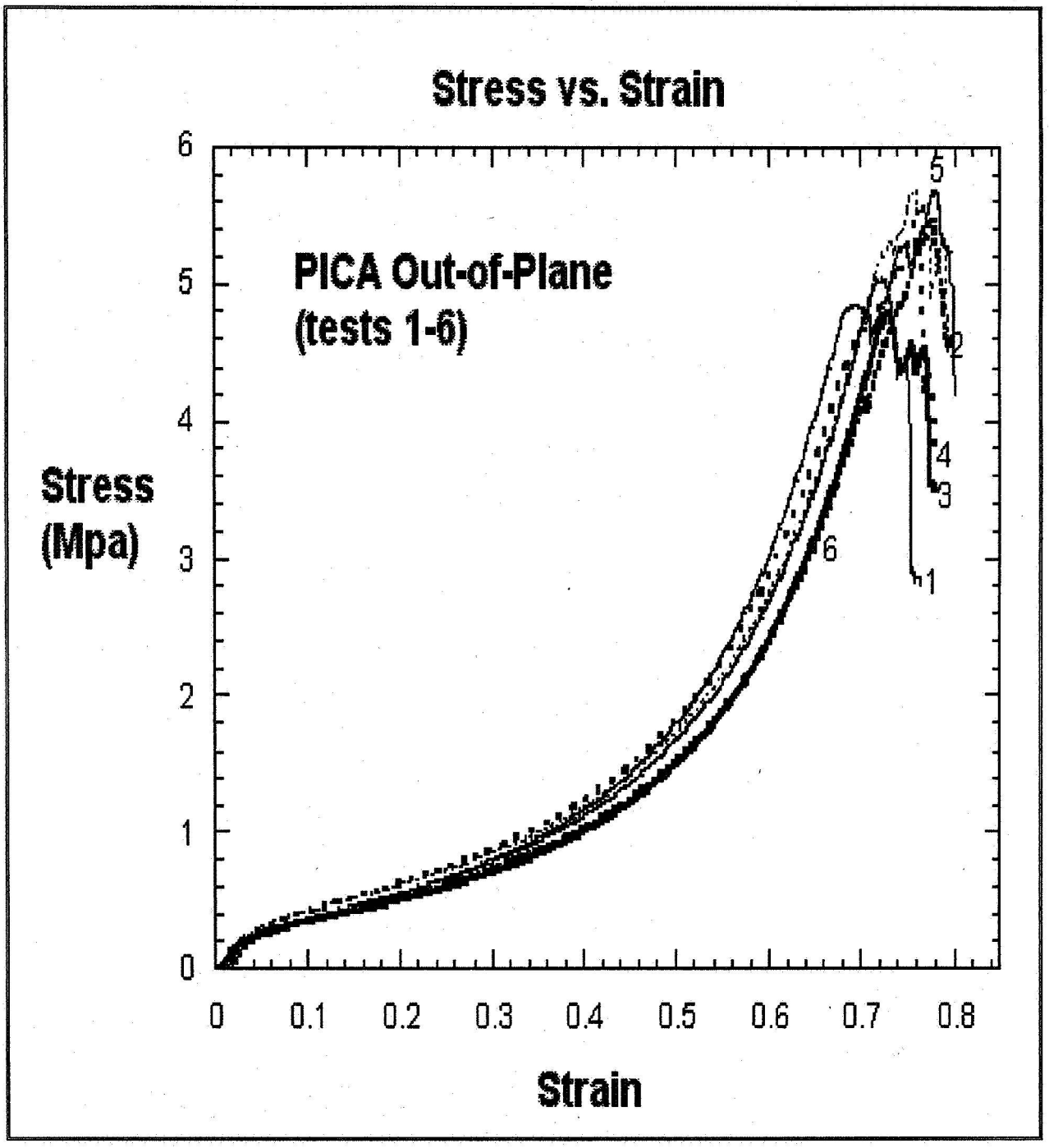

Figure 4.17
Representative stress-strain curves during compression testing of charred PICA in the in-plane direction. Tests #1-11 are shown.

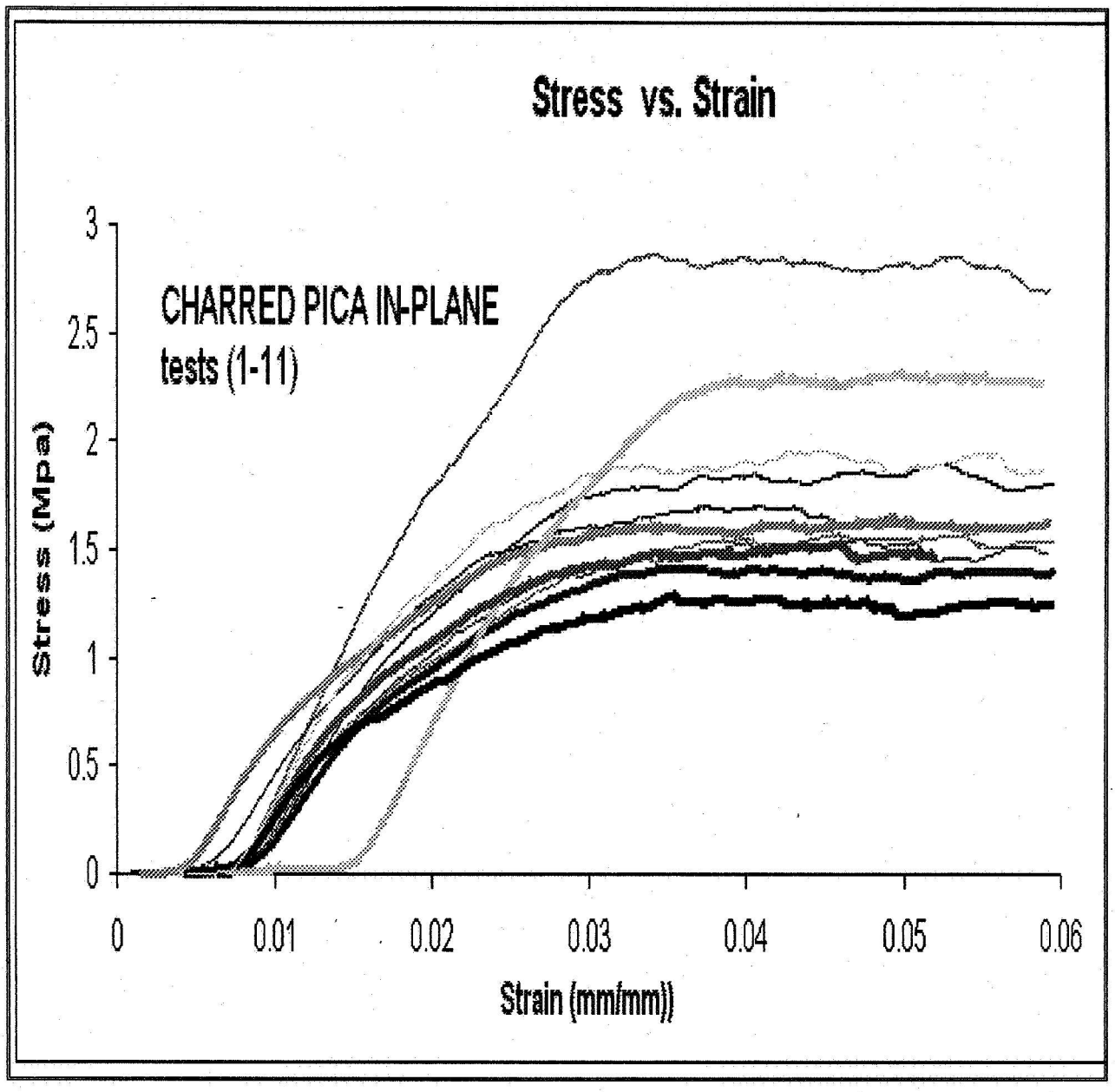

Figure 4.18
Representative stress-strain curves during compression testing of charred PICA in the out-of-plane direction. Tests #1-4 are shown.

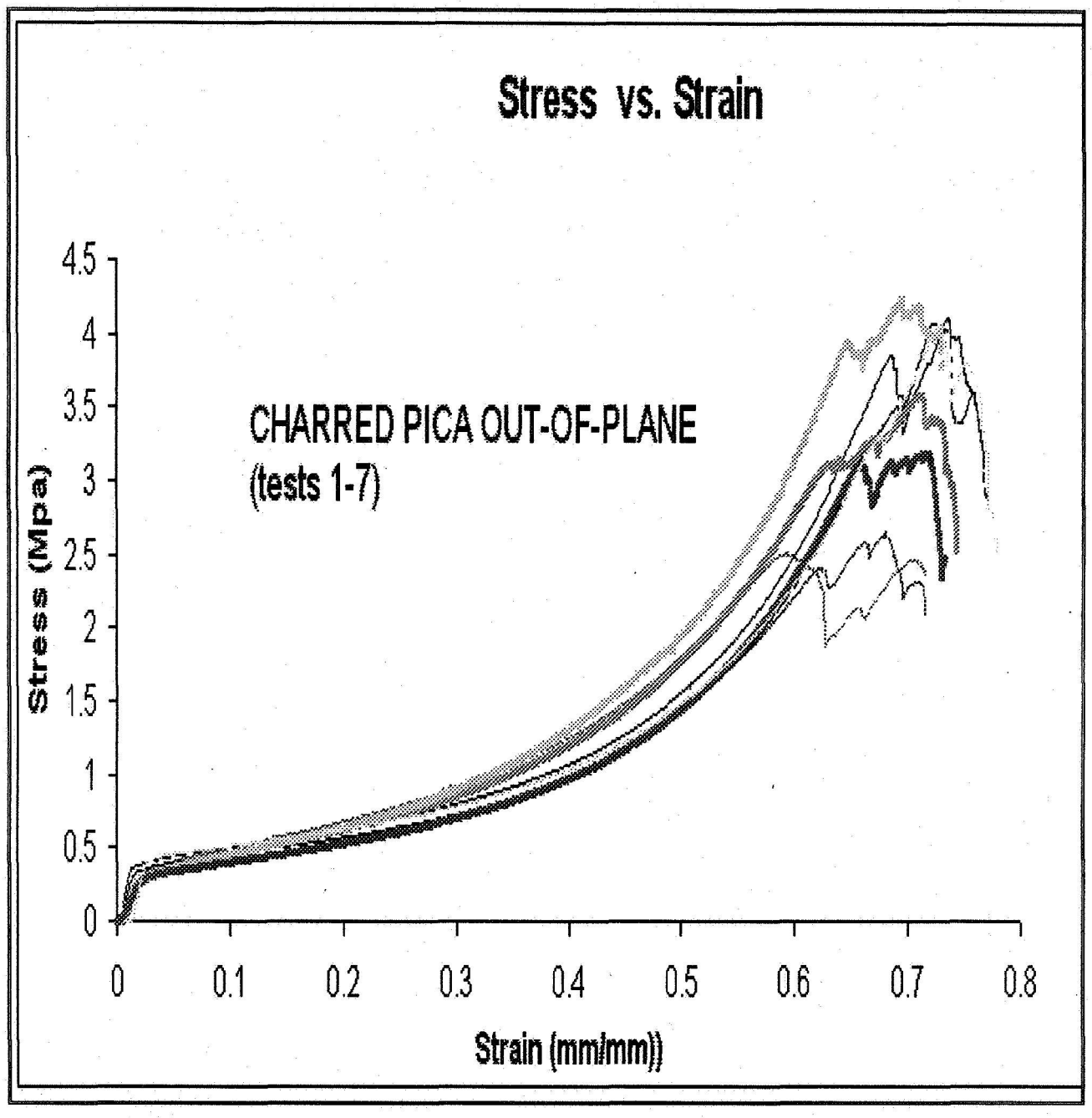

Figure 4.19
Early unloading during compression testing of PICA in the out-of-plane direction. Each curve is from a different specimen.

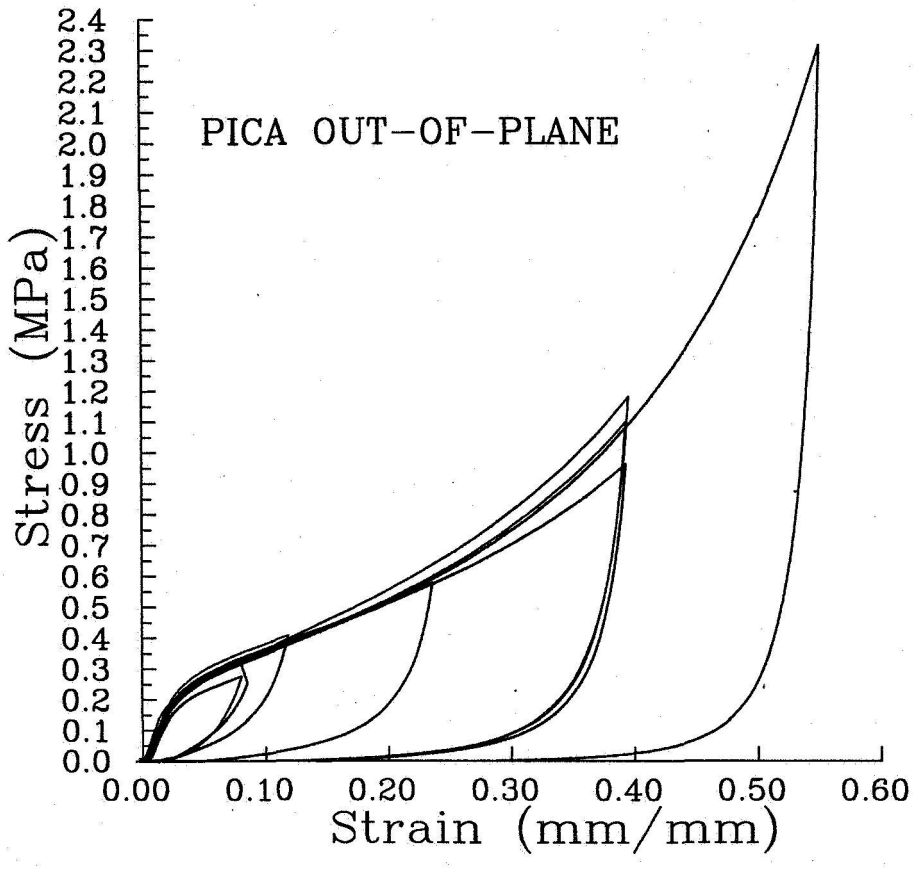

Figure 4.20
Effect of loading rate during compression testing of SIRCA 15A in the in-plane direction. The loading rate varies from 0.051 mm/min to 1.016 mm/min.

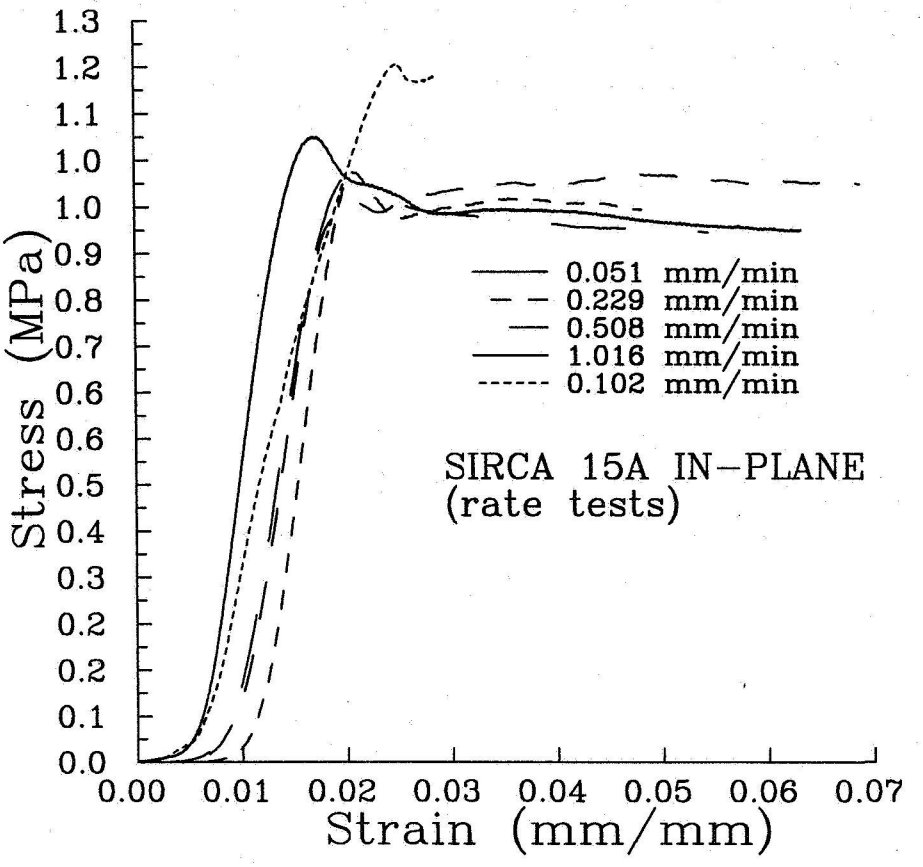

Figure 4.21
Effect of loading rate during compression testing of SIRCA 15F in the in-plane direction. The loading rate varies from 0.051 mm/min to 1.016 mm/min.

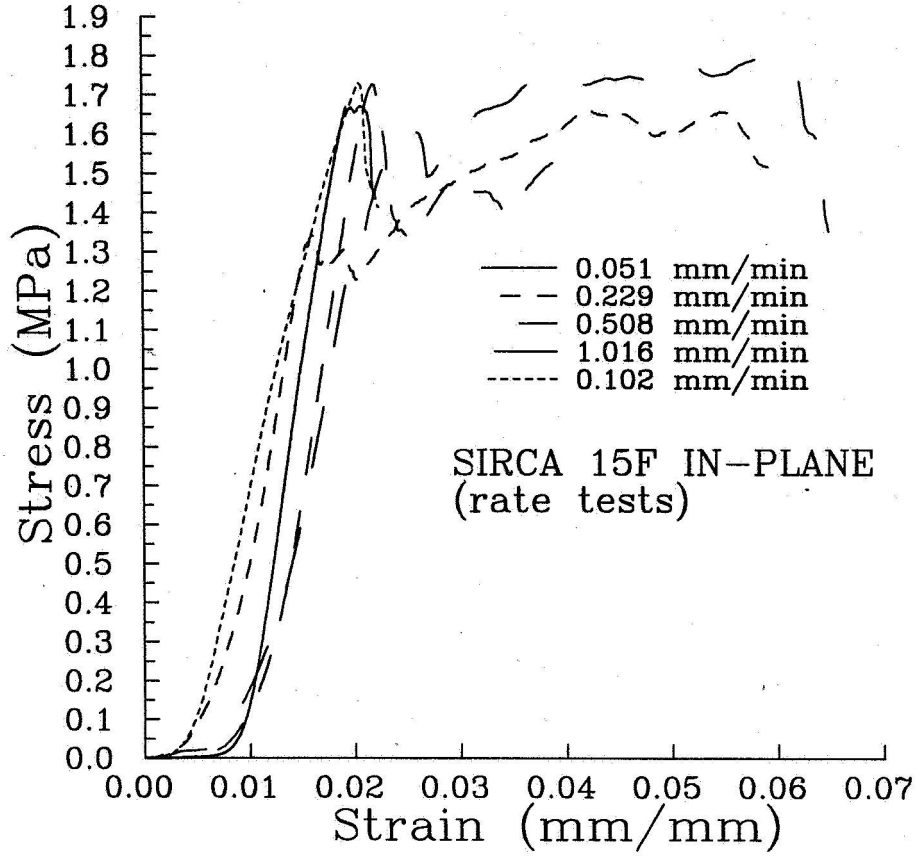

Figure 4.22
Effect of loading rate during compression testing of PICA in the in-plane direction. The loading rate varies from 0.051 mm/min to 1.016 mm/min.

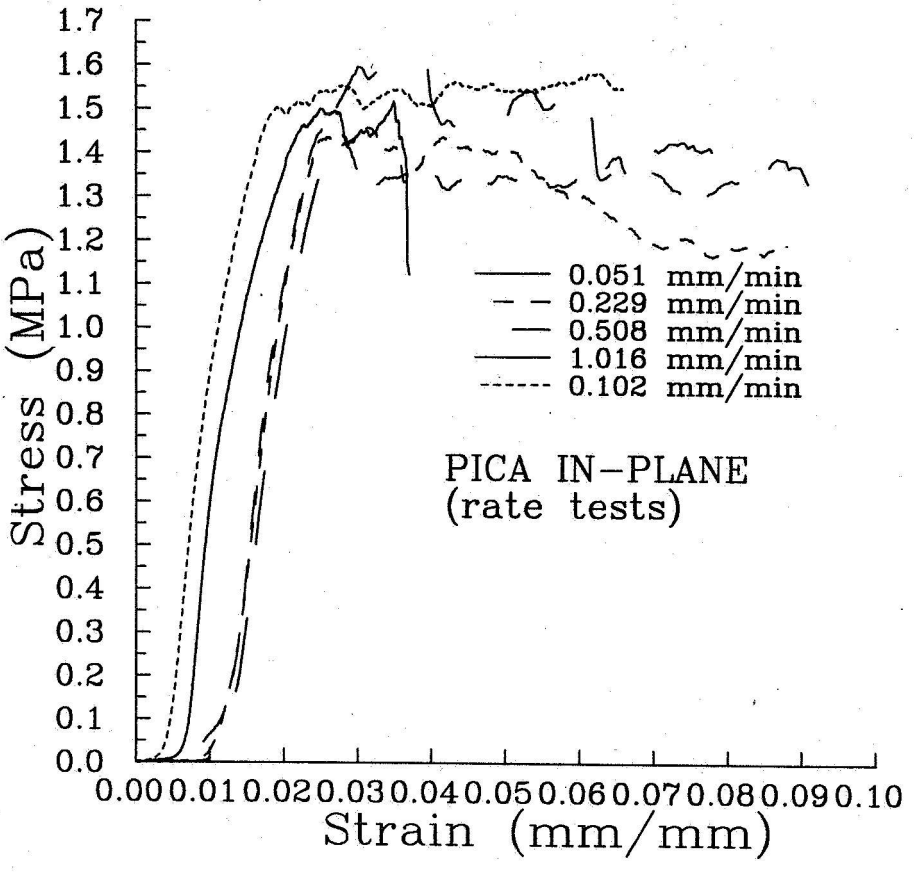

Figure 4.23
Failure Mode "Out-of-Plane"

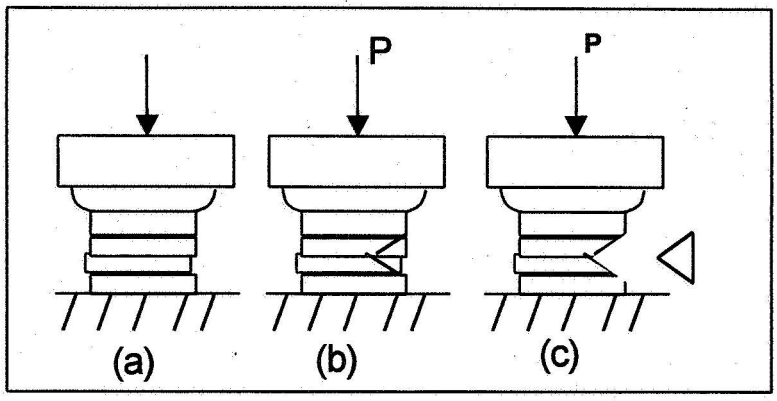

Figure 4.24
Failure Mode "In-Plane"

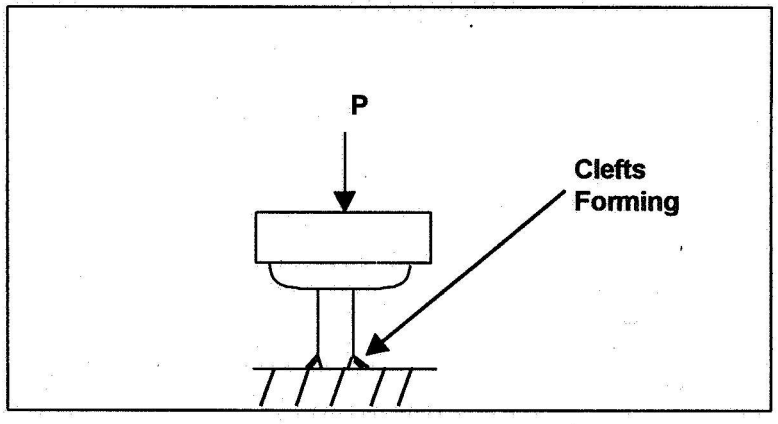

Chapter

5

Shear Testing

Another property that is important in establishing design parameters for LCA applications is the shear strength. The Iosipescu shear test procedure *(Iosipescu, [1963])* was followed to determine the shear strength of the LCA materials. Such tests were used earlier by Parmenter and Milstein *[1998]* in their study of the mechanical properties of fiber reinforced aerogels. In this procedure, notched beam specimens are loaded in antisymmetric four point bending on the *Instron 1123.* Figures 5.1 and 5.2 show the dimensions and loading arrangement, respectively, of an Iosipescu specimen. The load is measured with a compression load cell, and the displacement is determined from the Instron's internal displacement gage. The crosshead speed is set at 0.102 mm/min, and all experiments are conducted under ambient conditions. The shear force, V, in the center of the specimen, is calculated from the measured peak load, P, with Equation 5.1. The shear stress, τ, in the center of the specimen is the shear strength divided by the cross sectional area at the notch root (Equation 5.2). Equations 5.3 and 5.4 show the relationships between loads on the specimen, F1 and F2 (see Figure 5.2), and measured load, P.

$$V = P * (b-a) / (a+b) \quad (5.1)$$

$\tau = V / (t * w)$, where t is the height of the notch and w is the specimen thickness. (5.2)

$$F1 = P * b / (a+b) \quad (5.3)$$

$$F2 = P * a / (a+b) \quad (5.4)$$

Under the appropriate conditions, a specimen tested in this way will have virtually pure shear within the section of the notch-root axis. Since brittle materials typically fail in tension before they fail in shear, this type of test can yield a lower bound of the shear strength. That is, if the specimens tested behave as truly brittle materials, they will fail in a tensile-mode before their ultimate shear strength is reached, and thus the actual shear strength will be greater than the indicated shear strength at failure. Diagrams depicting Iosipescu specimens failing by pure shear and by tension are provided in Figure 5.3 and

5.4. A specimen failing by pure shear will exhibit cracking across the notch-root axis, as in Figure 5.3, whereas a specimen failing by tension will exhibit two areas of cracking outside of the notch-root axis in the pattern shown in Figure 5.4.

It was observed that a third failure scenario may result with fibrous materials when the specimens are oriented with fiber planes perpendicular to the notch-root axis (out-of-plane direction). Tensile cracks may begin to form at the top and bottom of the notch-root axis, and then propagate until impeded by fibers. Then, two new cracks may form, one below the top crack and one above the bottom crack, and they will propagate until impeded by fibers. This pattern continues until failure occurs. A diagram depicting an Iosipescu specimen failing in this manner is provided in Figure 5.5.

It was also observed that a fourth failure scenario may result with fibrous materials when the specimens are oriented with fiber planes parallel to the notch-root axis (in-plane direction). Vertical cracks may appear to the left and right of the notch-root axis, instead of at the center, and may propagate through the height of the specimen. This occurs if there are planes of weakness at locations other than the notch-root axis (where weakness is anticipated). The failure mode that results is a combination of shear and bending. A diagram of this scenario in provided in Figure 5.6.

"Charred" SIRCA 15A, virgin SIRCA 15F, as well as "charred" and virgin PICA materials were tested with the Iosipescu method. The "charred" materials underwent the uniform charring process in the pyrolyzing oven described in Chapter 2. Specimens oriented in the out-of-plane direction had fiber planes perpendicular to the notch-root axis. While specimens oriented in the in-plane direction had fiber planes parallel to the notch-root axis. The out-of-plane specimens failed by a series of tensile cracks along the notch root axis, as depicted in the failure scenario in Figure 5.5. As a result, calculations of shear strength by the Iosipescu approach yield a lower bound to the actual shear strength, as described above.

The in-plane specimens all failed off-center in two locations of weakness, as depicted by the scenario in Figure 5.6. As in the case of the out-of-plane specimens, the indicated shear strength as calculated by the Iosipescu method is really a lower bound to the actual shear strength.

Table 5.1 summarizes the shear test results. For virgin and charred materials of SIRCA 15A and PICA, the lower bounds of shear strength in the out-of-plane direction are twice

as large as those in the in-plane direction. SIRCA 15F tested in the out-of-plane direction had the highest lower bound of shear strength (0.51 MPa). Out-of-plane and in-plane shear results are compared with compressive strengths in Table 5.2. The compressive strengths for PICA are much higher than the lower bounds of shear strength in the in-plane and out-of-plane directions, with compressive strength to shear strength ratios of 16:1 for the in-plane direction and 27:1 for the out-of-plane direction.

During shearing tests it was observed that when the virgin SIRCA 15F materials fractured, their fracture was abrupt and the initial crack was able to propagate easily. After the fracture these specimens were no longer able to absorb energy. However, the PICA materials resisted crack propagation after the initial fracture had occurred. Although their shear strength may be less than that of other materials, such materials that resist crack propagation may be advantageous in certain designs. A calculation of the energy absorbed during shearing may be used to quantify this characteristic. This characteristic to resist crack propagation may be an indication of the bond strength between the fibers and the matrix. Tests such as "fiber pull out strength" are recommended to provide further insight to characterize the material's strength.

Figure 5.1
Diagram of dimensions of an Iosipescu shear test specimen.

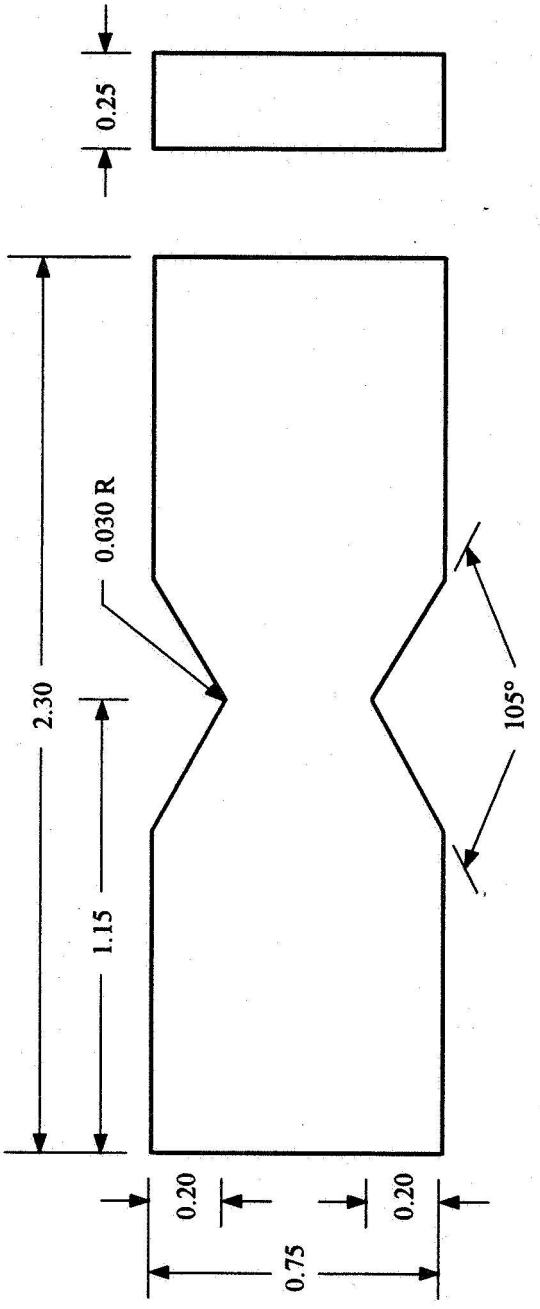

Figure 5.2
Diagram of loading arrangement of an Iosipescu specimen.

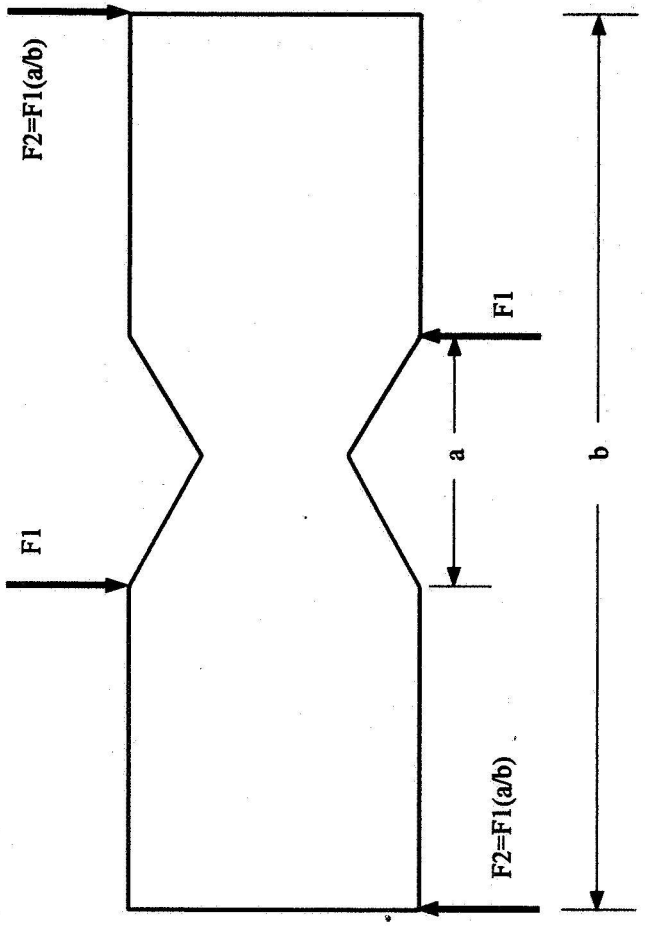

Figure 5.3
Diagram of an Iosipescu specimen failing by pure shear.

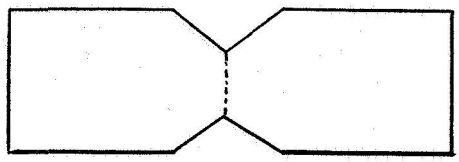

Figure 5.4
Diagram of an Iosipescu specimen failing by tension.

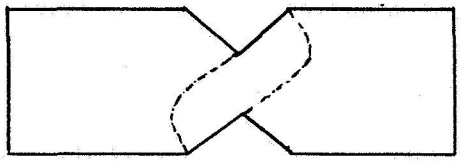

Figure 5.5
Diagram of failure mode for an Iosipescu specimen with fiber planes perpendicular to the notch-root axis

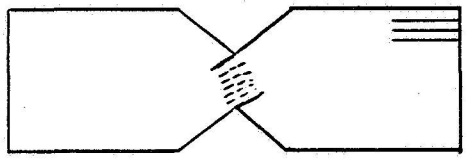

Figure 5.6
Diagram of failure mode for an Iosipescu specimen with fiber planes parallel to the notch-root axis

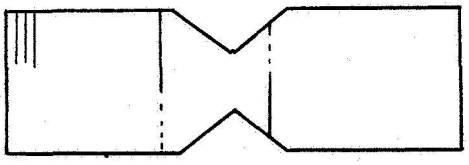

Table 5.1
Summary of Shear Test Results

Test #	Lower Bound of Shear Stress (MPa)						
	Charred SIRCA 15A in-plane	Charred SIRCA 15A out-of-plane	Virgin SIRCA 15F out-of-plane	Virgin PICA in-plane	Virgin PICA out of-plane	Charred PICA in-plane	Charred PICA out-of-plane
1	0.40	0.74	0.53	0.12	0.26	0.11	0.24
2	0.34	0.80	0.55	0.10	0.25	0.11	0.22
3	0.15	0.13	0.49	0.07	0.26	0.11	0.29
4	0.15	0.17	0.48	0.07	0.25	0.14	0.25
5	0.17	0.28	0.49	0.10	0.23	0.10	0.26
6	0.31	0.57	0.54	0.10	0.21	0.11	0.21
7	0.21	0.10	0.49	0.10	0.22	0.10	0.19
8	0.10		0.54	0.11	0.21	0.10	0.24
9	0.15		0.47		0.22	0.07	0.29
10	0.13				0.25		0.20
average	**0.21**	**0.40**	**0.51**	**0.10**	**0.24**	**0.11**	**0.24**
std dev	**0.10**	**0.28**	**0.03**	**0.02**	**0.02**	**0.02**	**0.03**

Table 5.2
Comparison of Shear and Compressive Strengths for LCAs

Material	Lower Bound of Shear Strength, τ (MPa)	Compressive Strength, σ (MPa)	Ratio of Compressive Strength to Shear Strength
Charred SIRCA 15A in-plane	0.21	1.51	7
Charred SIRCA 15A out-of-plane	0.40	1.20	3
Virgin SIRCA 15F out-of-plane	0.51	NA	NA
Virgin PICA in-plane	0.10	1.55	16
Virgin PICA out-of-plane	0.24	6.41	27
Charred PICA in-plane	0.11	1.79	16
Charred PICA out-of-plane	0.24	3.54	15

Chapter

6

Scanning Electron Microscopy

Scanning electron microscopy work has been initiated to enable a greater understanding of the LCA materials' microstructure in the in-plane and out-of-plane directions, and to view fracture surfaces of samples that had undergone mechanical testing. Micrographs of fracture surfaces can often yield information about failure mechanisms. Observations of the differences between PICA, SIRCA 15A and SIRCA 15F in the virgin state, and in the charred state, are also of interest. The electron microscopy work in this project is in its initial stage. An important goal of the microscopy study is to compare virgin and charred specimens of each LCA material in the in-plane and out-of-plane directions at equivalent magnifications. This includes viewing free surfaces, machined surfaces, and fracture surfaces. The fracture surface images should include in-plane and out-of-plane views for both in-plane and out-of-plane mechanical tests, including compression, tension, and shear fracture surfaces. For example, for a compression specimen tested in the in-plane direction, the resulting fracture surface should be viewed in both the in-plane and out-of-plane directions.

Initial microscopy work focused on fracture surfaces of compression specimens tested in both in-plane and out-of-plane directions. Since scanning electron microscopes (SEMs) require materials that are electrically conductive (and LCA's are not) the specimens viewed were coated with gold-palladium prior to insertion into the SEM chamber. Images of six compression specimens are included in this report.

The first fracture surface is a portion from an in-plane compression test specimen of charred SIRCA 15A. The surface was viewed parallel to the fiber planes. Figure 6.1 shows a schematic diagram of the fracture surface and the direction from which it was viewed. Figure 6.2 is an image of the surface taken at a magnification of X6000. The predominant fiber in this image has a smooth end, and does not appear to be fractured as a result of testing. The "flaky" material around the fibers may be residue of the silicone infiltrant resulting from the pyrolysis process. It may also be crushed pieces of material resulting from compression testing. Future comparisons of charred SIRCA 15A surfaces before and after loading should yield further information.

The second fracture surface is from an out-of-plane compression test specimen of charred SIRCA 15A. The fracture surface was viewed perpendicular to the fiber planes. Figure 6.3 is a diagram illustrating the fracture surface and viewing direction. Figures 6.4 through 6.7 show images at magnifications of X250, X750, X2300, and X4300. Figure 6.5 shows a strange "bubble" feature. Figure 6.6 shows a nice view of a curved silica fiber. All images show the same "flaky" material mentioned above. In Figure 6.2, the end of a fiber is seen to have a rather smooth appearance; in Figure 6.7, fibers with jagged ends are seen. To date, no microscopy work has been done on virgin SIRCA 15A. It will be of interest, in due course, to compare the appearances of virgin and charred surfaces of SIRCA 15A.

The third and fourth fracture surfaces are from two different out-of-plane compression test specimens of SIRCA 15F. In both cases the surfaces were viewed parallel to the fiber planes. Figure 6.8 shows a schematic diagram of the first SIRCA 15F fracture surface and viewing direction. Figures 6.9 through 6.13 are images at magnifications of X25, X100, X500, X1800, and X2700. Figure 6.14 illustrates the second SIRCA 15F fracture surface and the direction from which it was viewed. Figures 6.15 through 6.18 show magnified images at X900, X4300, and two at X10000. All of the images for SIRCA 15F show more webbing of the silicone infiltrant, and fewer "flaky" bits of material than observed in the charred SIRCA 15A images. Figures 6.12 and 6.13 show individual fibers with smooth ends; Figure 6.11 shows the same fibers at a lower magnification. Figures 6.17 and 6.18 show the silicone coating on individual fibers, with some degree of separation or "peeling." Images of charred surfaces and surfaces viewed perpendicular to the fiber planes are not yet available for SIRCA 15F.

The fifth fracture surface is a portion from an in-plane compression test specimen of PICA. The surface was viewed perpendicular to fiber planes. Figure 6.19 is a schematic illustration of the fracture surface and the viewing direction. Figure 6.20 is an image at X4500 magnification, and Figure 6.21 consists of 4 images at various lower magnifications. Figure 6.20 shows a nice view of a fiber that may or may not have been fractured during the compression test. In these images the PICA material has a much more porous microstructure, and less webbing of the infiltrant, than for the case of SIRCA 15F.

The final fracture surface is from a different in-plane compression test specimen of PICA. Once again, the surface was viewed perpendicular to the fiber planes. Figure 6.22 illustrates the fracture surface and direction from which it is viewed. Figures 6.23 through

6.26 show images at magnifications of X15, X25, X100, and X750. These images show a greater presence of the phenolic infiltrant than for the case above, and the phenolic has a much more "crusty" appearance. This difference may be due to uneven impregnation of the phenolic. Such variations in color and texture of PICA are also apparent to the naked eye. No microscopy results are yet available for surfaces viewed parallel to the fiber planes, or for charred PICA.

Preliminary microscopy results have yielded interesting images at a wide range of magnifications. Microscopy work should be continued to obtain images of in-plane and out-of-plane fracture surfaces of charred and virgin materials of all types, from all different types of mechanical tests, and at angles parallel and perpendicular to the fiber planes. Electron microscopy images of the FRCI, AIM, and Fiberform substrates should be taken. In addition, free surfaces and machined surfaces should be compared with fracture surfaces. Comparisons of such a full range of photomicrographs should allow conclusions to be drawn concerning failure mechanisms (e.g., do individual fibers fracture or "pull-out" of the polymer matrix during a particular mode of failure), porosity *(Marschall and Milos [1998]; Marschall and Cox [1999])*, and charring effects.

Figure 6.1
Schematic diagram of a charred SIRCA 15A test specimen after compression in the in-plane direction. The fracture surface and direction of viewing during microscopy are indicated by arrows. The photomicrograph is shown in Figure 6.2.

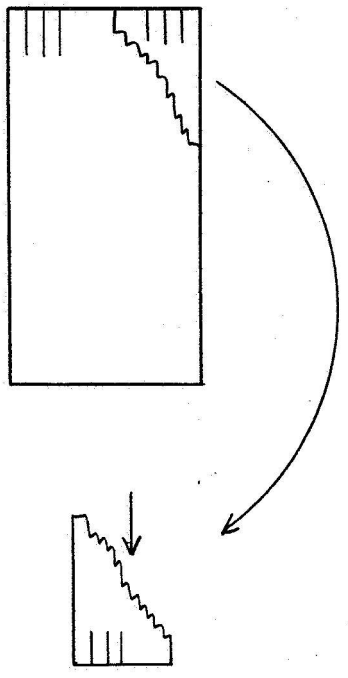

Figure 6.3
Schematic diagram of a charred SIRCA 15A test specimen after compression in the out-of-plane direction. The fracture surface and direction of viewing during microscopy are indicated by arrows. The photomicrographs are shown in Figures 6.4 through 6.7.

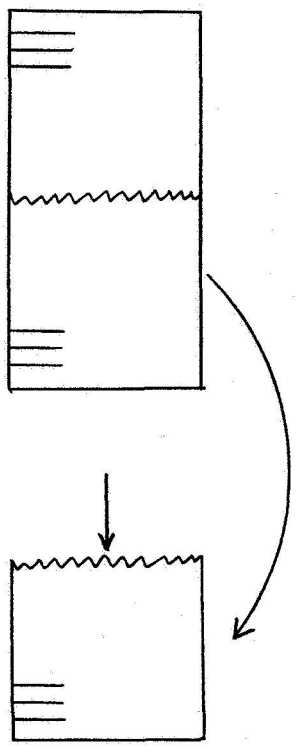

Figure 6.8
Schematic diagram of a SIRCA 15F test specimen after compression in the out-of-plane direction. The fracture surface and direction of viewing during microscopy are indicated by arrows. The photomicrographs are shown in Figures 6.9 through 6.13.

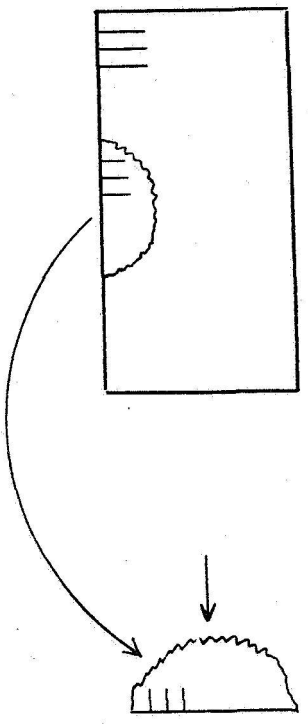

Figure 6.14
Schematic diagram of a SIRCA 15F test specimen after compression in the out-of-plane direction. The fracture surface and direction of viewing during microscopy are indicated by arrows. The photomicrographs are shown in Figures 6.15 through 6.18.

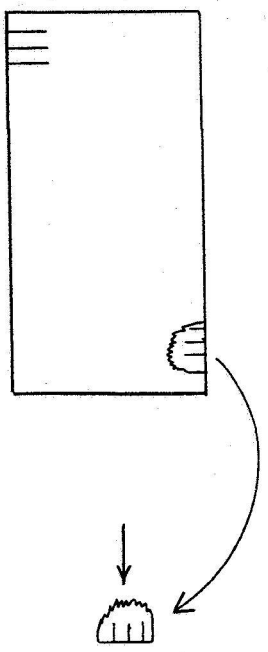

Figure 6.19
Schematic diagram of a PICA test specimen after compression in the in-plane direction. The fracture surface and direction of viewing during microscopy are indicated by arrows. The photomicrographs are shown in Figures 6.20 and 6.21.

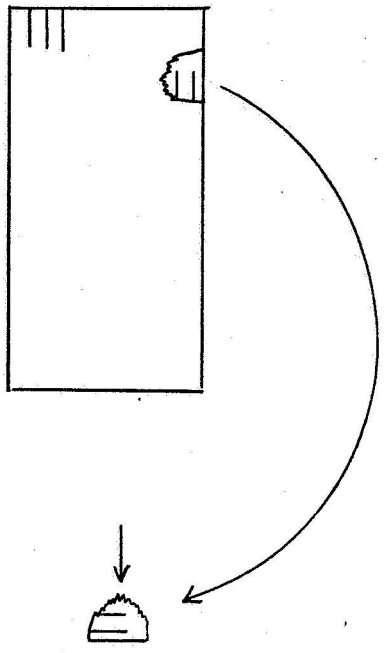

Figure 6.22
Schematic diagram of a PICA test specimen after compression in the in-plane direction. The fracture surface and direction of viewing during microscopy are indicated by arrows. The photomicrographs are shown in Figures 6.23 through 6.26.

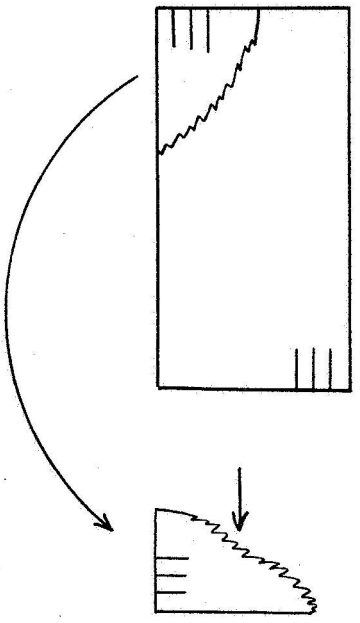

Chapter

7

Conclusions and Recommendations

The first phase of mechanical testing of LCAs has been completed and the results are provided in the preceding chapters. Experiments conducted to date include hardness, compression, and shear tests on SIRCA 15A, SIRCA 15F and PICA, and hardness tests on AIM, FRCI, and Fiberform. Both charred and virgin materials were tested. Additionally, electron microscopy studies were started, and the initial results are presented.

Hardness results for the virgin LCA materials in the in-plane and out-of-plane directions, and the charred materials in the out-of-plane direction, are fairly complete. However, a study in which the hardness is measured as a function of processing variables should also be done to determine the influence of variations in the material properties from one "batch" to the next. In addition, more extensive hardness testing of charred material is necessary to verify initial results and to determine the influence of char depth on hardness.

Extensive compression testing of charred and virgin SIRCA 15A, SIRCA 15F, and PICA has been carried out and the results are presented. The characteristic responses of each material, under both "in-plane" and "out-of-plane" loading, were determined. During in-plane compressive loading, the materials fail by an apparent "separation and buckling" mechanism. By contrast, under out-of-plane compression, the materials undergo significant, highly nonlinear, plastic (i.e., permanent) deformation, wherein the stress (and its rate of change) increases with increasing strain. Considerable energy is absorbed during out-of-plane compression. This behavior is readily understood from microstructural considerations.

In future tests, particular care needs to be given to documenting all processing variables. As an example, three batches of SIRCA 15F yielded somewhat different average compressive strengths (i.e., 1.44, 1.64, and 2.08 MPa – see Tables 4.6 and 4.7). The difference between the different batches of material shows the need to test specimens from a large number of batches to determine the ranges of scatter. Combined hardness and compression testing on such a range of materials should also provide a basis for

establishing a firm correlation between hardness and compressive strength. In addition, compression tests of the AIM, FRCI, and Fiberform fibrous substrates would be useful for comparison with their impregnated counterparts to see how much of each composite's strength is attributed to the fibrous substrate, and how much results from impregnation. The compressive responses of the substrate materials should be compared with the results of the respective hardness measurements, which have already been made on the substrates.

Shear tests yielded lower bounds of shear strength. Since these materials failed in non-shear modes (i.e., tension and/or bending), the actual shear strength is higher than the strength indicated in test results. Shear tests should be expanded to include tests of virgin SIRCA 15A (in-plane and out-of-plane), virgin SIRCA 15F (in-plane), and charred SIRCA 15F (in-plane and out-of-plane).

Scanning electron microscopy work has been initiated to enable a greater understanding of the LCA materials' microstructure in the in-plane and out-of-plane directions, and to view fracture surfaces of samples that have undergone mechanical testing. A number of fracture surfaces, over a range of magnifications, up to 10,000X, are included in this report. The initial microscopy results have yielded interesting images at a wide range of magnifications. Microscopy work should be continued to obtain images of in-plane and out-of-plane fracture surfaces of charred and virgin materials of all types, from all different types of mechanical tests, and at angles parallel and perpendicular to the fiber planes. Electron microscopy images of the FRCI, AIM, and Fiberform substrates should be taken. In addition, free surfaces and machined surfaces should be compared with fracture surfaces. Comparisons of such a full range of photomicrographs should allow conclusions to be drawn concerning failure mechanisms (e.g., do individual fibers fracture or "pull-out" of the polymer matrix during a particular mode of failure), porosity *(Marschall and Milos [1998]; Marschall and Cox [1999])*, and charring effects.

In addition to the tests mentioned above, several other experiments are recommended. These include tension, bending, torsion, and fatigue tests on the fibrous substrates, the LCAs, and pyrolyzed material. These tests should be combined with studies of microstructural features of undeformed material, of plastically deformed material, and of fracture surfaces (under tension, compression, shear, and fatigue) using both optical and scanning electron microscopes, as discussed above. To date, all mechanical testing was done in an "in-plane" or "out-of-plane" manner. Tests should also be done to characterize the mechanical response when the load is applied over a range of orientations, say at θ =

30°, 45°, and 60°, wherein θ is the angle between the fiber planes and the direction of loading. Novel tests including "fiber pull out strength" to gain information about the fiber/matrix bonding, nano-hardness of the matrix and fibers separately, and tests of the cohesion of the fibers to one another (melting of aluminaborosilicate) would also be of interest to develop. In due course, tests of mechanical behavior should also be carried out at elevated temperatures.

On the theoretical side, we recommend work on the development of fundamental models of the mechanical properties of LCAs, including the properties of the protective char-layer and the bonding of the char-layer to the bulk material. The experimental data that are reported herein will provide a basis for developing theoretical understanding and modeling of the mechanical behavior of the LCAs. As a first step, we suggest seeking both empirical and theoretical relationships among the various mechanical properties and micro- and macro-structural features of the materials.

References

Georgeson, G. and F. Milstein, Nuclear Instruments and Methods A285 (1989) 507.

Iosipescu, N., Rev. Mec. Appl. 1 (1963) 147.

James, K., V. Gerrish, E. Cross, J. Markakis, J. Marschall, and F. Milstein, Nuclear Instruments and Methods A322 (1992).

James T. W. and F. Milstein, J. Materials Science 18 (1983) 3249.

Johnson, C., NASA Ames Research Center, Personal Communication, 1999.

Kim, K. and F. Milstein, Construct. Building Materials 1 (1987) 209.

Marschall, J. and F. S. Milos, Journal of Thermophysics and Heat Transfer 12 (1998) 1.

Marschall, J. and M. E. Cox, "Gas Permeability of the Lightweight Ceramic Ablators PICA and SIRCA," 1999 to be published.

Parmenter, K. E. and F. Milstein, Journal of Non-Crystalline Solids 223 (1998) 179-189.

Schieber, M., C. Ortale, L. van den Berg, W. Schnepple, L. Keller, C.N.J. Wagner, W. Yelon, F. Ross, G. Georgeson, and F. Milstein, Nuclear Instruments and Methods A285 (1989) 172.

Tran, H. K., "Development of Lightweight Ceramic Ablators and Arc Jet Test Results," NASA TM 108798, January 1994.

Tran, H. K., C. Johnson, D. Rasky, F. Hui, Y.-K. Chen, and M. Hsu, "Phenolic Impregnated Carbon Ablators (PICA) for Discovery Class Missions," AIAA 96-1911, June 1996.

Tran, H. K., C. Johnson, D. Rasky, F. Hui, and M. Hsu, "Silicone Impregnated Reusable Ceramic Ablators for Mars Follow-on Missions," AIAA 96-1819, June 1996.

Tran, H. K., M. Smith, D. Tran, T. Castellano, M.-T. Hsu, T. Chen, C. E. Johnson, D. M. Smith, I. Terraza-Salinas, D. Alter, D. Paragas, and L. Kobayashi, "Mars/Pathfinder Back Interface Plate Heat Shield and Designs Verification Tests in the Ames 20MW Panel Test Facility," Mars/Pathfinder Project Office of the Jet Propulsion Laboratory, December 1995.

Tran, H. K., C. E. Johnson, M.-T. Hsu, M. Smith, H. Dill, and A. Chen-Jonsson, "Qualification of the Forebody Heatshield of the Stardust's Sample Return Capsule," AIAA 97-2482, June 1997.

Tran, H. K. et al., "Phenolic Impregnated Carbon Ablators (PICA) as Thermal Protection Systems for Discovery Missions," NASA TM 110440, 1997.